



**HAL**  
open science

## Microseismicity and faulting geometry in the Gulf of Corinth (Greece)

Denis Hatzfeld, Vassilis Karakostas, Maria Ziazia, Iannis Kassaras, Elephteria Papadimitriou, Kostas Makropoulos, Nikos Voulgaris, Christos Papaioannou

► **To cite this version:**

Denis Hatzfeld, Vassilis Karakostas, Maria Ziazia, Iannis Kassaras, Elephteria Papadimitriou, et al.. Microseismicity and faulting geometry in the Gulf of Corinth (Greece). *Geophysical Journal International*, 2000, 141, pp.438-456. 10.1046/j.1365-246X.2000.00092.x . insu-03606314

**HAL Id: insu-03606314**

**<https://insu.hal.science/insu-03606314>**

Submitted on 11 Mar 2022

**HAL** is a multi-disciplinary open access archive for the deposit and dissemination of scientific research documents, whether they are published or not. The documents may come from teaching and research institutions in France or abroad, or from public or private research centers.

L'archive ouverte pluridisciplinaire **HAL**, est destinée au dépôt et à la diffusion de documents scientifiques de niveau recherche, publiés ou non, émanant des établissements d'enseignement et de recherche français ou étrangers, des laboratoires publics ou privés.



Distributed under a Creative Commons Attribution 4.0 International License

# Microseismicity and faulting geometry in the Gulf of Corinth (Greece)

Denis Hatzfeld,<sup>1</sup> Vassilis Karakostas,<sup>2</sup> Maria Ziazia,<sup>3</sup> Iannis Kassaras,<sup>3</sup> Eleftheria Papadimitriou,<sup>2</sup> Kostas Makropoulos,<sup>3</sup> Nikos Voulgaris<sup>3</sup> and Christos Papaioannou<sup>2</sup>

<sup>1</sup>Laboratoire de Géophysique Interne et Tectonophysique, UJF-CNRS, BP 53, 38041 Grenoble Cedex 9, France

<sup>2</sup>Geophysical Department, Aristotle University, BP 352–01, 54006, Thessaloniki, Greece

<sup>3</sup>Department of Geophysics, University of Athens, Illissia, 15784 Athens, Greece

Accepted 1999 December 6. Received 1999 December 6; in original form 1999 May 7

## SUMMARY

During the summer of 1993, a network of seismological stations was installed over a period of 7 weeks around the eastern Gulf of Corinth where a sequence of strong earthquakes occurred during 1981. Seismicity lies between the Alepohori fault dipping north and the Kaparelli fault dipping south and is related to both of these antithetic faults. Focal mechanisms show normal faulting with the active fault plane dipping at about 45° for both faults. The aftershocks of the 1981 earthquake sequence recorded by King *et al.* (1985) were processed again and show similar results. In contrast, the observations collected near the western end of the Gulf of Corinth during an experiment conducted in 1991 (Rigo *et al.* 1996), and during the aftershock studies of the 1992 Galaxidi and the 1995 Aigion earthquakes (Hatzfeld *et al.* 1996; Bernard *et al.* 1997) show seismicity dipping at a very low angle (about 15°) northwards and normal faulting mechanisms with the active fault plane dipping northwards at about 30°. We suggest that the 8–12 km deep seismicity in the west is probably related to the seismic–aseismic transition and not to a possible almost horizontal active fault dipping north as previously proposed. The difference in the seismicity and focal mechanisms between east and west of the Gulf could be related to the difference in the recent extension rate between the western Gulf of Corinth and the eastern Gulf of Corinth, which rotated the faults dipping originally at 45° (as in the east of the Gulf) to 30° (as in the west of the Gulf).

**Key words:** focal mechanisms, Gulf of Corinth, microseismicity, shallow faulting.

## INTRODUCTION

Different mechanisms are involved during lithospheric extension within a continental environment. The two extreme mechanisms are: (1) distributed deformation and thinning of the lithosphere as a whole (pure shear) (e.g. McKenzie 1978); and (2) faults that cut the lithosphere (simple shear) (e.g. Wernicke 1985). It seems generally accepted now that the subcrustal lithosphere and lower crust deform in a ductile manner and that seismically active faults affect only the upper brittle crust (e.g. Jackson & White 1989). The geometry of the faults affecting the upper crust is, however, still a matter of debate. Some authors do not think that faults dipping at an angle of less than 30° are seismologically active (e.g. Jackson 1987), while others assume that parts of normal faults could dip at

very low angles (less than 15°), similar to the almost horizontal surfaces separating granitic basement from tilted sedimentary cover as seen in metamorphic core complexes (Wernicke 1995).

The various models proposed are, however, related to different types of observations. No large earthquakes are related to shallow-dipping normal faults (Jackson & White 1989), even though one exception was observed for an earthquake in Papua New Guinea, a region deforming at a very fast rate (Abers *et al.* 1997). Also, using body wave modelling, a shallow-dipping fault was proposed for the latest subevents that constitute the main shocks of the 1981 Corinth earthquake (King *et al.* 1985; Jackson *et al.* 1982) or of two Turkish earthquakes (Eyidogan & Jackson 1985), but a more detailed study (Braunmiller & Nabelek 1996) showed that the results were controversial.

On the other hand, low-angle normal faults are commonly observed in the field (Wernicke 1995) and in seismic reflection profiles (Allmendiger *et al.* 1983). The controversial question is therefore: are the very-low-angle ( $5^{\circ}$ – $10^{\circ}$ ) faults active (and possibly aseismic), or are they the result of rotation around a horizontal axis (Jackson & White 1989; Wernicke 1995)?

Another question is related to the segmentation of normal faults. Usually, the dimensions along the strike of normal faults do not exceed 20–25 km (Jackson & White 1989), which implies an upper limit for the magnitude of the earthquakes that can occur on individual fault segment. However, it is not clear whether the discontinuities separating the different segments are stable and will never break, or if occasionally the rupture can jump from one segment to another, thereby leading to an earthquake of greater magnitude (Jackson & White 1989).

This paper presents (or summarizes when already published) the results relating to the fault geometry of the Gulf of Corinth obtained during several microseismicity and aftershock surveys.

## GEOLOGICAL BACKGROUND

The Aegean (Fig. 1) is a region of fast-moving, widespread extensional deformation (Jackson 1994) located between the two lithospheric plates of Eurasia and Africa, which converge at a rate of about  $1 \text{ cm year}^{-1}$  (DeMets *et al.* 1990). The total extension across the Aegean is about  $4\text{--}5 \text{ cm year}^{-1}$  as deduced

from satellite geodesy (Reilinger *et al.* 1997), and it probably started around the Miocene period (Mercier *et al.* 1976). This extensional deformation involves most of the Aegean from the north Aegean Trough, to the Hellenic Trench in a complex pattern of strike-slip and normal faults. One of the most prominent active structures follows the Gulf of Corinth, which separates Continental Greece from the Peloponnese (McKenzie 1978). The Gulf of Corinth, which has experienced several destructive earthquakes in recent decades, has been the location of recent extensive geological, geodetic and seismological studies.

## Seismicity

Instrumental seismicity of the Aegean clearly shows a strong concentration of earthquakes around the Gulf of Corinth (Figs 1 and 2). One of the last strong sequences of events occurred in 1981, and was extensively studied (Jackson *et al.* 1982; King *et al.* 1985; Bezzeghoud *et al.* 1986; Taymaz *et al.* 1991; Abercombie *et al.* 1995; Hubert *et al.* 1996). Other destructive earthquakes occurred more recently in the western Gulf of Corinth (Fig. 2) near Galaxidi (Hatzfeld *et al.* 1996), Aigion (Bernard *et al.* 1997) and Patras (Karakostas *et al.* 1994). This high level of activity is also attested by the historical seismicity (Ambraseys & Jackson 1990, 1997; Papazachos & Papazachou 1997), which includes several earthquakes of magnitude greater than 6 around the Gulf of Corinth. Most of the computed focal mechanisms of strong events indicate

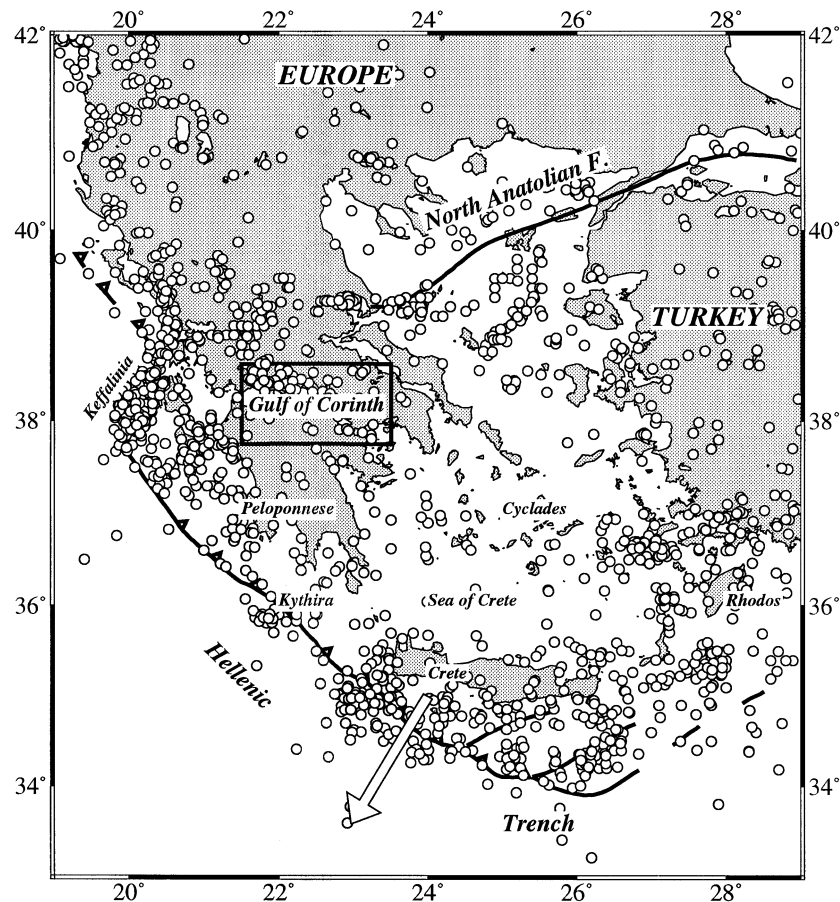


**Figure 1.** General sketch of the Aegean showing the main features and geographical names. The open circles are the NEIS earthquakes of magnitude greater than 4.5 located between 1963 and 1996. The white arrow is the motion of the Aegean relative to Europe (Le Pichon *et al.* 1995).

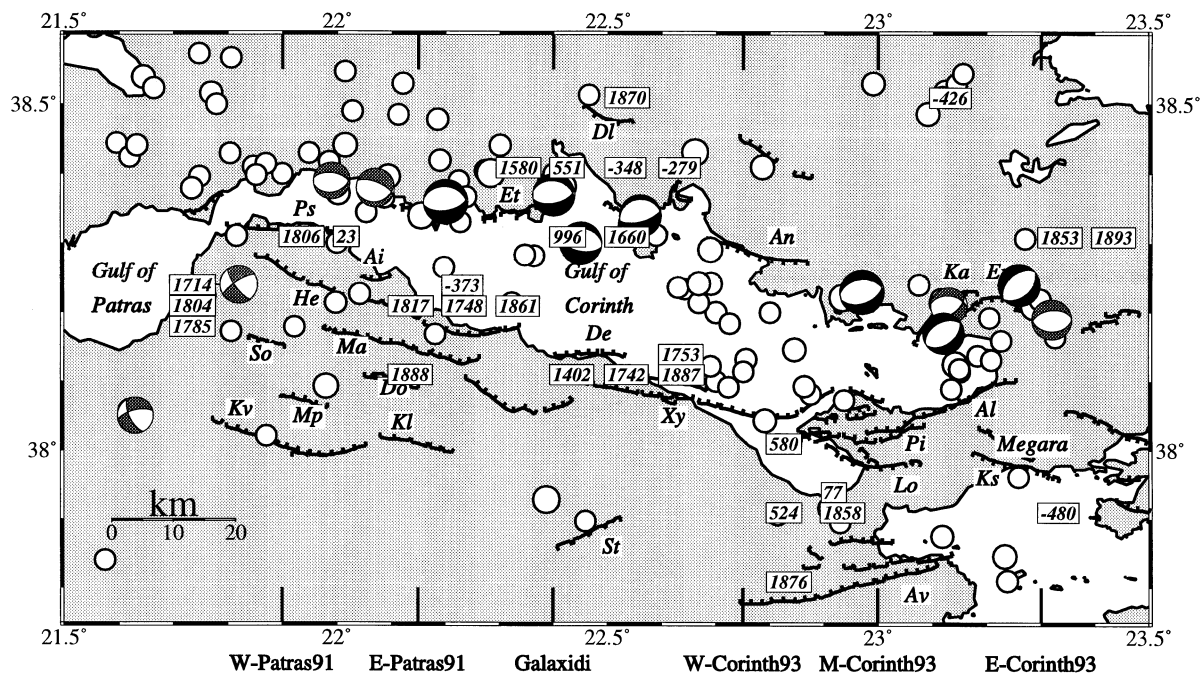


**Figure 2.** Main tectonic features of the Gulf of Corinth. Historical seismicity (Papazachos & Papazachou 1997) is reported in boxes; instrumental seismicity (NEIC, magnitude > 4.5) and focal mechanisms of the strongest earthquakes are computed by body wave modelling and Harvard CMT solutions. The main faults (after Rigo *et al.* 1996) are indicated: Ai, Aigion; Ps, Psathopyrgos; So, Sotena; Mp, Mega Pontias; Kv, Kato-Vlasia; He, Helike; Ma, Mamoussa; Do, Doumena; Kl, Kalavrita; Dl, Delphi; De, Derveni; Xy, Xylokaastro; An, Antikira; Av, Agios-Vasilleos; Lo, Loutraki; Pi, Pisias; Al, Alepohori; Ka, Kaparelli, Er, Erithres; Ks, Kakia-Skala; St, Stymfalia. The cross-sections refer to Fig. 12.

normal faulting with a N–S-trending extension (Jackson 1987; Taymaz *et al.* 1991; Hatzfeld *et al.* 1996; Bernard *et al.* 1997; Baker *et al.* 1997) as is also the case for microearthquake mechanisms (Hatzfeld *et al.* 1990; Rigo *et al.* 1996).

### Tectonics

The Gulf is in the general shape of an asymmetric half-graben with the southern footwall being uplifted (Roberts *et al.* 1993; Armijo *et al.* 1996). A series of three main faults, the Psathopyrgos, the Helike and the Xylokaastro faults, dipping north and striking E–W, bound the southern margin of the Gulf. Their lengths of about 25 km suggest a limitation of the maximum magnitude of earthquakes associated with a single fault segment of  $M_w = 6.7$  (Roberts & Jackson 1991). Some smaller sized antithetic faults can be found on the northern coast of the Gulf. They are more extensive at the eastern end of the Gulf (the Loutraki and the Kaparelli faults) but also exist in the centre (the Delphi, Erithres and Antikira faults). The western end of the Gulf of Corinth is connected through the Rio–Antirio strait to the Gulf of Patras, which does not have any major faults comparable to those affecting the Gulf of Corinth. The eastern end of the Gulf of Corinth truncates the Megara basin through a complex pattern of faults with a more NE–SW strike (Leeder *et al.* 1991). Faults also affect the deepest part of the Gulf, which is located underwater (Brooks & Ferentinos 1984). The total extension rate of the faults known from GPS measurements is about  $10 \text{ mm yr}^{-1}$ . It is not clear, however, if part of the uplift is due to regional uplift (Collier 1990; Mariolakos & Stiros 1987) or if it is due to a

flexural process only (Armijo *et al.* 1996). The map of the active faults at the surface is generally well accepted, but the geometry with depth is not so clear, and faults of listric shape (Poulimenos *et al.* 1989; Doutsos & Piper 1990), an almost flat seismologically active zone (Rigo *et al.* 1996) and faults connected to the lower crust with ductile deformation (Armijo *et al.* 1996) have been proposed to accommodate the deformation. Further south, other apparently inactive faults have been mapped (Fig. 2) that suggest that active faulting moved northwards recently.

### Deformation

The deformation of the Gulf of Corinth has been measured by comparing GPS measurements with old triangulations conducted in 1890 or between 1966 and 1972 (Billiris *et al.* 1991; Clarke *et al.* 1997; Davies *et al.* 1997; Briole *et al.* 1999). The N–S extension is about  $15 \text{ mm yr}^{-1}$  in the western part of the Gulf around Rio, and about  $10 \text{ mm yr}^{-1}$  in the eastern part of the Gulf of Corinth around Corinth. A comparison between several GPS surveys measured over a shorter duration gives slightly higher extension values, but with the same difference between the western and eastern ends of the Gulf. It therefore seems clear that the present deformation is faster around Rio than around Corinth. This deformation is relatively well confined in the centre of the Gulf on a very narrow deforming zone. Depending on the method of estimating the seismic energy released over the last century, it would appear that strong earthquakes are overdue in the western Gulf of Corinth (Clarke *et al.* 1997).

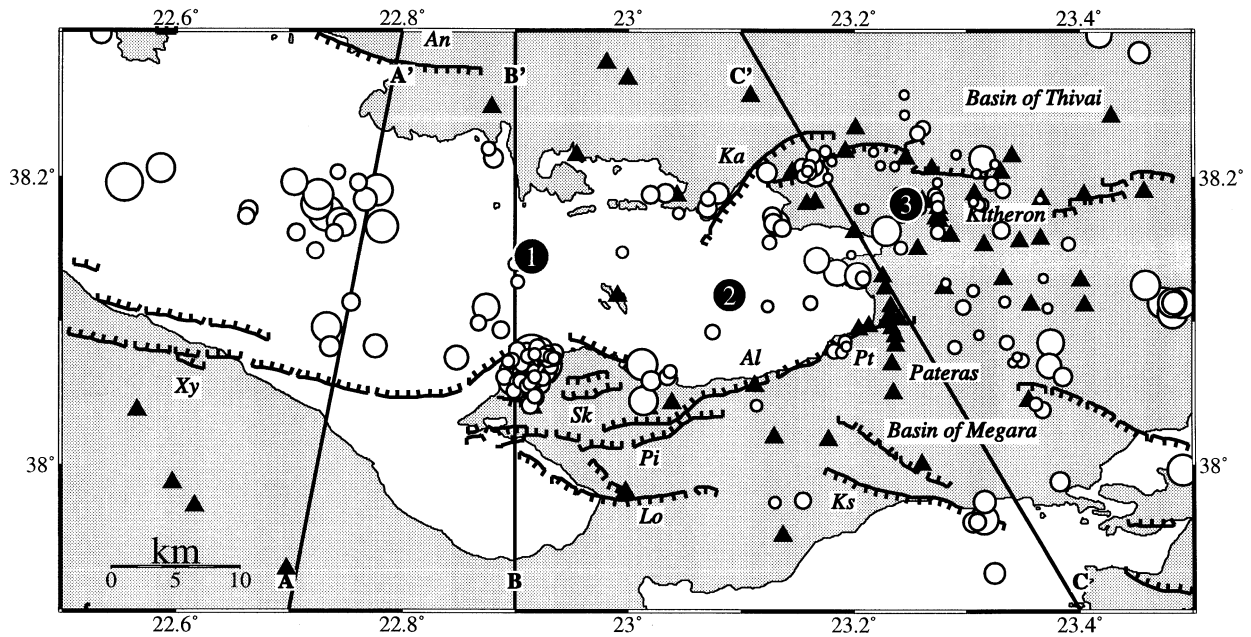


**Figure 3.** Map of the 232 earthquakes (recorded by more than 12 stations with an rms error  $< 0.3$  s and errors in location  $< 3$  km) recorded during the summer of 1993. Open circles are epicentres; black triangles are seismological stations. Faults are the same as in Fig. 2. The three cross-sections of Fig. 5 are indicated. The relocated epicentres of the three main shocks of 1981 are also shown (Taymaz *et al.* 1991).

Several questions arise from this brief review. (1) Are all the faults active or is it mostly the faults that bound the Gulf to the south that are active? (2) What is the geometry of the faults with depth? (3) Are the faults segmented and how are they connected? (4) Do the eastern and western parts of the Gulf respond to the same process?

This paper presents and summarizes the results of various microseismicity experiments and aftershock studies conducted around the Gulf of Corinth. The results of an experiment conducted around the eastern part of the Gulf of Corinth

in 1993 are presented first. The results are then compared with those obtained by reprocessing the data of the aftershock survey of the 1981 earthquake conducted by King *et al.* (1985). Other parts of the Gulf of Corinth are examined, together with data collected during a microearthquake survey of the western part of the Gulf (Rigo *et al.* 1996) and during aftershock studies of the Galaxidi earthquake of 1992 November 18 (Hatzfeld *et al.* 1996), the Patras earthquake of 1993 July 14 (Karakostas *et al.* 1994) and the Aigion earthquake of 1995 June 15 (Bernard *et al.* 1997).

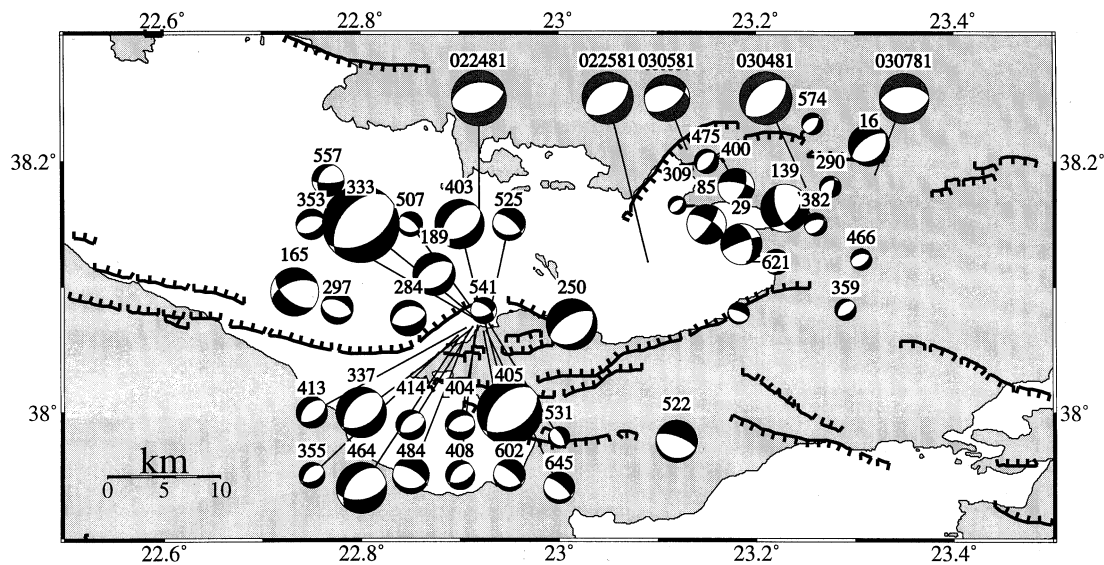


**Figure 4.** Map of the 33 focal mechanisms computed during summer 1993. The size of the beachball is proportional to the magnitude. The focal mechanisms of the strong earthquakes in Fig. 2 are also shown, with compressional quadrants in grey.

Seismicity maps are presented showing cross-sections of seismicity perpendicular to the major faults. Because the inferred geometry of active faults based on seismicity alone may be biased by the depth variation of the brittle–ductile transition, the projection of fault planes of all mechanisms is also presented (selecting the active fault plane from the seismicity).

## EAST CORINTH 1993

### Data

In order to resurvey the area of the 1981 earthquakes a temporary network of portable stations was installed around the east of the Gulf of Corinth (Fig. 3). During the summer of 1993 (from July 17 to August 25) 36 smoked-paper Sprengnether MEQ 800 stations (for the last time!) and 18 Reftek digital data loggers were installed. This network was complemented by a dozen digital stations that were installed in order to assess site effects and topographical effects (Fig. 3). The average spacing between stations was about 10 km to ensure earthquake depth accuracy. More than 11 000 *P* phases and 16 000 *S* phases were used to locate 670 events recorded by more than four stations. To locate the events the velocity structure and  $V_p/V_s$  ratio of Rigo *et al.* (1996) were adopted. Details regarding the procedure usually adopted to locate the most reliable earthquakes can be found in previous papers (e.g. Hatzfeld *et al.* 1990). Among the 450 events, 232 (including a cluster) were recorded by more than 12 stations, and located with an rms error of less than 0.3 s, and with uncertainties of less than 3 km for both epicentre and depth (Fig. 3). In addition, 39 focal mechanisms were computed for earthquakes with more than eight first-motion polarities of upgoing rays (Fig. 4).

### Seismicity

Most of the seismicity (Fig. 3) is located between the Xylokaastro and Alepohori faults to the south and the Kaparelli fault to the north. This seismicity continues eastwards and seems to be restricted to the Pateras and Kithiron mountains located between the two basins of Megara and Thivai. Most of the seismicity is not clearly associated to the Kaparelli, Alepohori, Pisia or Xylokaastro faults, which were supposed to be related to the 1981 earthquakes (Jackson *et al.* 1982; Hubert *et al.* 1996). During the experiment, a moderate earthquake of magnitude  $M_l = 3.6$  occurred ( $38.07^\circ\text{N}$ ,  $22.90^\circ\text{E}$ ). It was located at a depth of 7 km, north of the Pisia fault, and was followed by about 120 aftershocks all located within a 5 km radius (Figs 3 and 5).

Several sections (Fig. 5) were plotted across the eastern part of the Gulf of Corinth that strike perpendicular to the main faults at the surface; they show that most of the seismicity is located between 4 and 13 km depth. The western section (Fig. 5A) is perpendicular to the Xylokaastro fault and clearly shows that the rather few events are probably related to the former fault dipping north and not to the Antikira antithetic fault located on the opposite side of the Gulf and dipping south.

The middle section (Fig. 5B) strikes perpendicular to the Pisia and Alepohori faults, across the strongest event and the associated cluster of aftershocks, during our experiment. It is

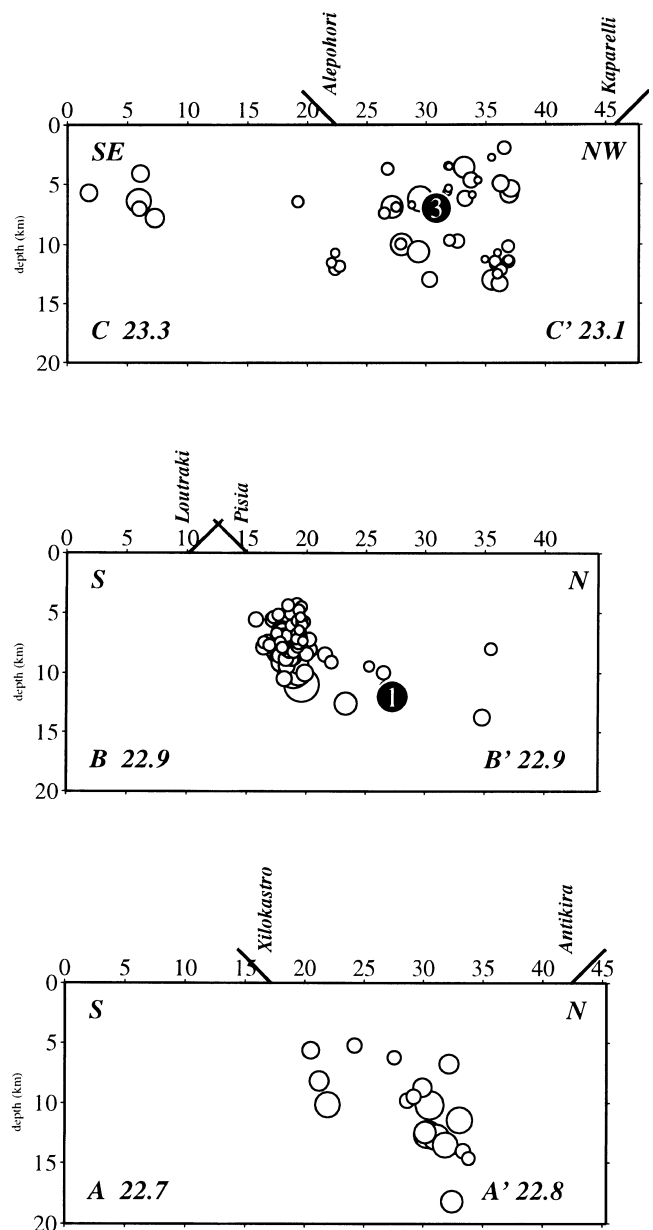


**Figure 5.** Cross-sections across the eastern Gulf of Corinth. The traces of the faults at the surface are indicated. Two of the three main shocks of 1981 (Taymaz *et al.* 1991) are shown.

suggested that this was the location of the first of the two earthquakes of February 1981 (Jackson *et al.* 1982; King *et al.* 1985; Taymaz *et al.* 1991; Hubert *et al.* 1996) and not the Xylokaastro fault as proposed by Abercombe *et al.* (1995).

The eastern cross-section (Fig. 5C) strikes perpendicular to the Kaparelli and Pateras faults and shows that the seismicity seems to dip south and is probably related to the Kaparelli fault, which was active during the last earthquake of the 1981 sequence on March 4. This last cluster is not obvious, however, and seismicity is more diffuse eastwards beneath the mountains.

### Focal mechanisms

Most of the 39 fault plane solutions computed during the experiment (Fig. 4) show extensional mechanisms very similar

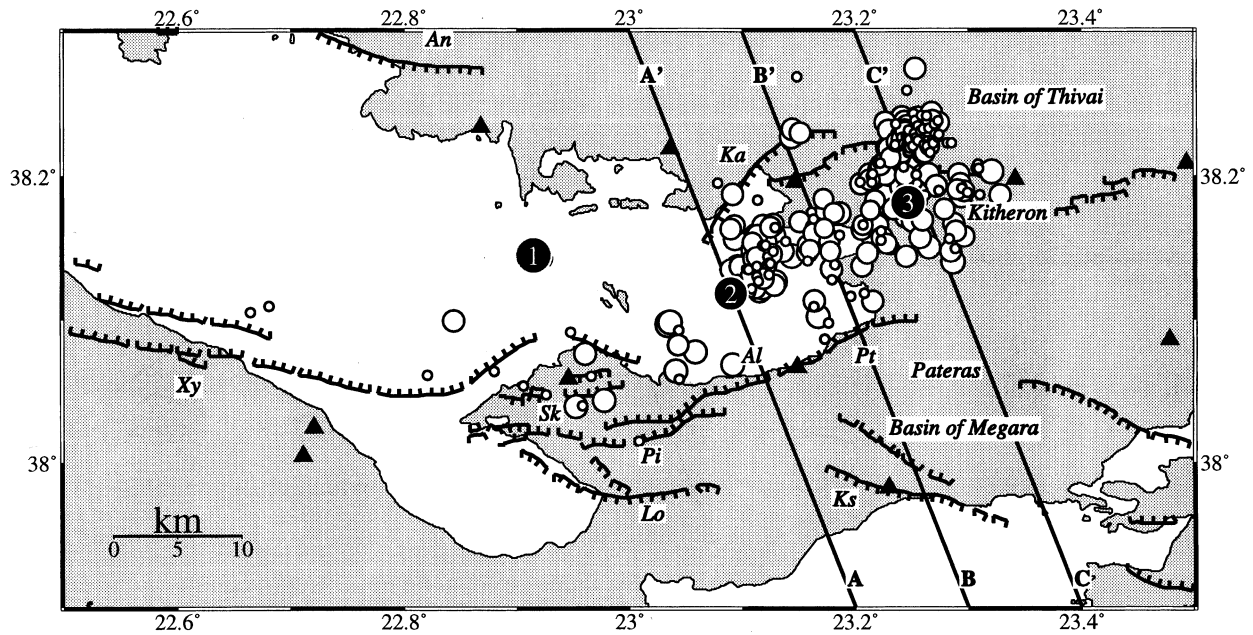


Figure 6. Map of the 350 strongest aftershocks recorded after the third event of 1981, on March 4, at more than 10 stations with an rms error <0.3 s and errors in location <3 km. The three main shocks are shown (Taymaz *et al.* 1991). The black triangles indicate seismological stations (King *et al.* 1985). The locations of the three cross-sections of Fig. 7 are indicated.

to the mechanisms of the three 1981 main shocks, with the T-axes trending NNW–SSE (Jackson *et al.* 1982; Bezzeghoud *et al.* 1986; Taymaz *et al.* 1991; Abercombie *et al.* 1995). In the eastern part, some strike-slip mechanisms are noted (#29, 85, 460) that are still consistent with N–S extension.

It therefore seems likely that the western seismicity is related to faults that dip towards the NNW (Xylokastro and Pisia) and is consistent with NNW–SSE extension, while the eastern seismicity, beneath the Kitheron mountain, is more complex but still consistent with NNW–SSE extension.

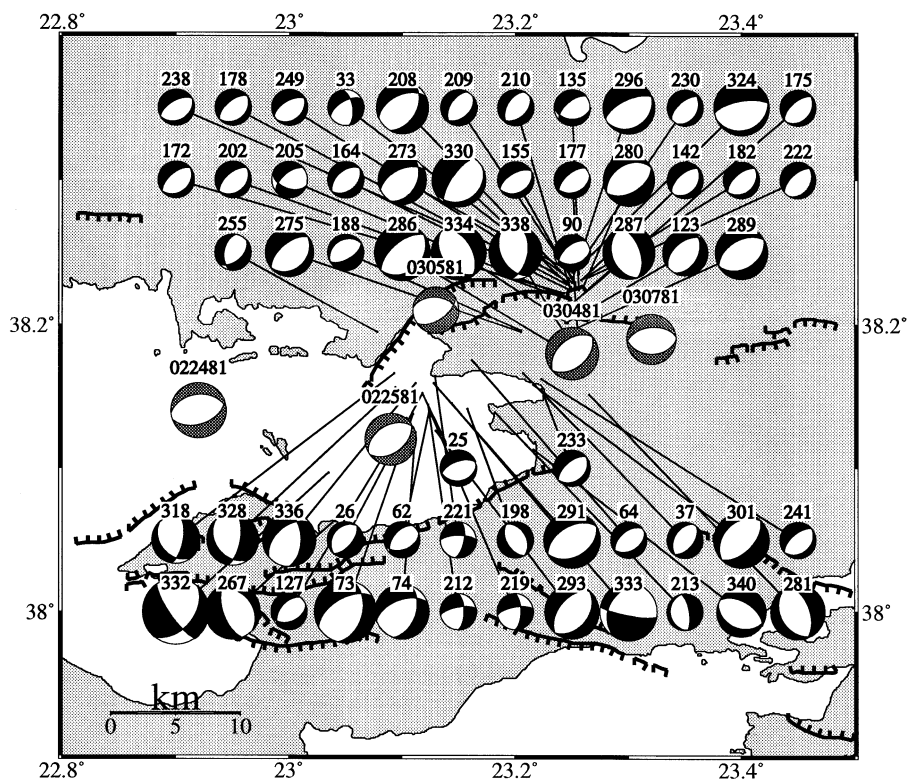


Figure 7. Focal mechanisms computed for 60 aftershocks of the 1981 East Corinth earthquakes. The focal mechanisms of the strongest events of Fig. 2 are shown in grey.

## EAST CORINTH 1981

## Data

In order to compare these results of 1993 with the 1981 earthquakes sequence, the records gathered by King *et al.* (1985) were reprocessed. More arrival times were read and the same locating procedure as for the 1993 data set was used. In 1981, the network consisted of 14 stations surrounding the main shock area with a spacing between stations of about 15 km. The installation of the stations started on 5 March 1981, that is, after the third event, which occurred on March 4. The arrival times relating to the 350 events considered to be amongst the largest in magnitude were read. Of the 350 events, 295 were recorded by more than 10 stations, located with an rms error of less than 0.3 s and an uncertainty of less than 3 km in epicentre and depth. These selected events are shown in Fig. 6.

## Seismicity

Most of the aftershock seismicity (Fig. 6) is located east of the Gulf and is confined between the Kaparelli and Alepohori faults. Only a few aftershocks were located to the west, beneath the Perahora peninsula, where the Pisia Fault is located, and could be related to the first two main shocks of the 1981 sequence. The aftershocks located in this survey (which were the strongest events in the series) are mostly related to the third event, which occurred on March 4 two weeks later; this survey presumably missed early aftershocks in the west that occurred before the network installation.

Three sections trending perpendicular to the Alepohori and Kaparelli faults and to the strike of the main shock fault planes were plotted (Fig. 8). Again, most of the seismicity ranged between depths of 4 and 14 km, similar to the 1993 experiment. In the west (Fig. 8A), the possibility of the seismicity being related to the Alepohori or the Kaparelli faults cannot be ruled out. In the centre of the cluster (Fig. 8B), a complex pattern of seismicity dipping both north and south is observed, suggesting that both the Alepohori and the Kaparelli faults are seismically active together. Eastwards (Fig. 8C), across the third event of March 4, a complex pattern of seismicity dipping both southwards and northwards is again found. This may possibly be related to the Platae Fault or to the Kaparelli Fault.

In none of the cross-sections is there evidence of a possible decrease in dip with depth for the north-dipping fault that could be related to a décollement located to the north (King *et al.* 1985).

## Focal mechanisms

60 focal mechanisms were computed with more than 10 first-motion polarities on the focal sphere (Fig. 7). Most of them are clearly similar to the mechanisms of the March 4 event computed by Jackson *et al.* (1982) and Taymaz *et al.* (1991). A few events show normal faulting, however, with a slight difference in the orientation of the T-axis. It is not clear whether this is related to some complexity in the stress pattern, given that the orientation of the T-axes for some solutions is determined by only one reading, or to heterogeneity in the velocity structure that could induce an uncertain solution.

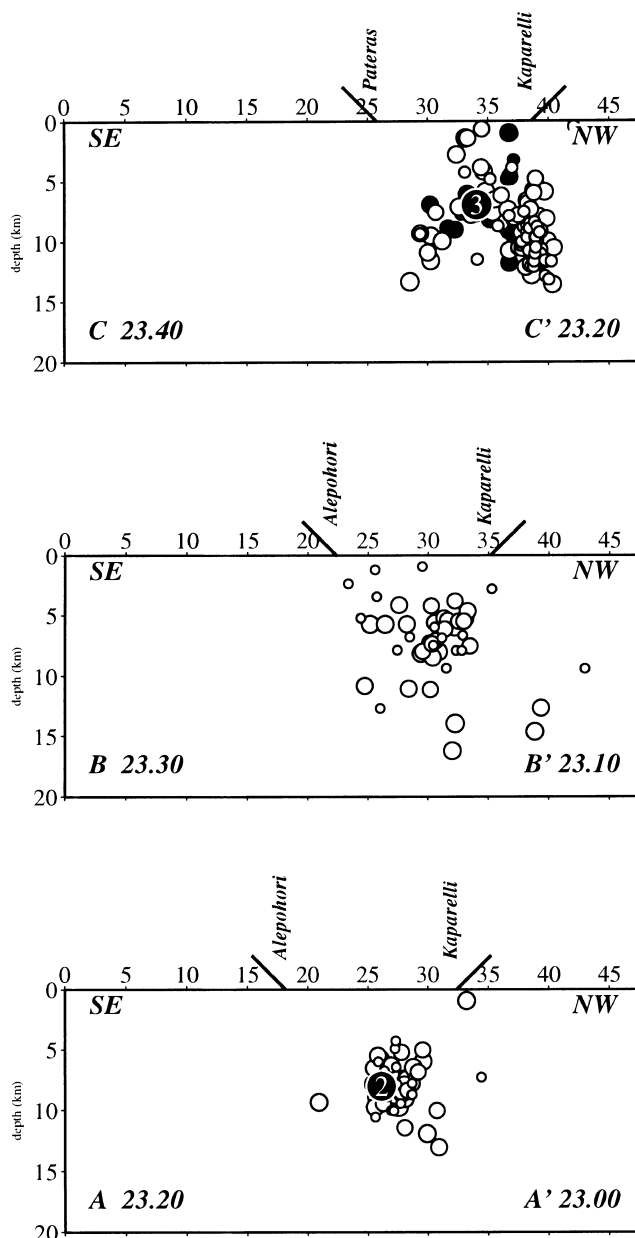


**Figure 8.** Cross-sections across the eastern Gulf of Corinth. Their locations are indicated in Fig. 6. The western section suggests that the Alepohori is the active fault, but the eastern cross-section shows that both the Kaparelli and the Alepohori faults are active. The main shocks are also indicated. In (C) aftershocks denoted by filled and open circles are located southwest and northeast of  $CC'$ , respectively. The aftershock distribution does not help in choosing between southeast- and northwest-dipping faults as the rupture plane of the third main shock of the 1981 events.

Here again there is no evidence of any change in the dip of the active fault plane with depth.

## PATRAS 1991

This experiment, conducted during July and August 1991 and involving more than 65 seismological stations, is described in great detail elsewhere (Rigo *et al.* 1996). In this paper a more complete set of data is presented, because we include the data

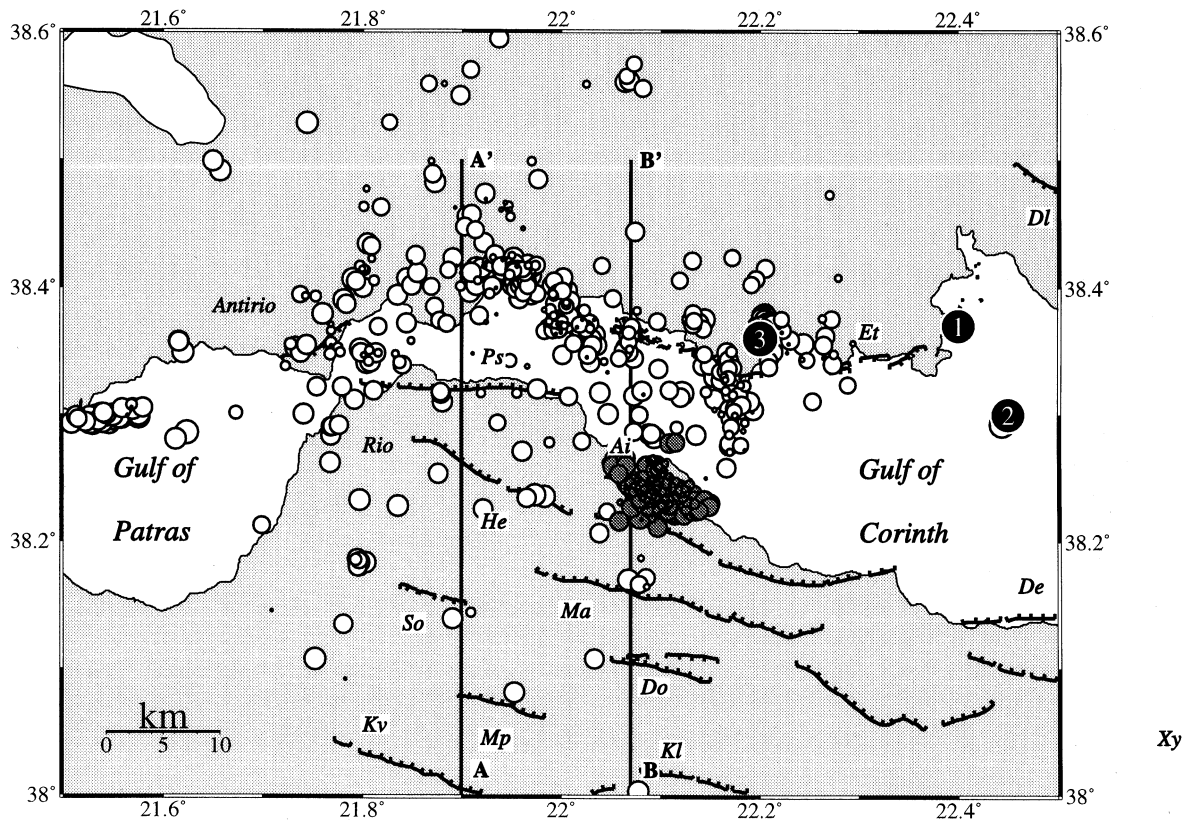


Figure 9. Map of the seismicity recorded during July and August 1991 around Patras at more than eight stations with an rms error  $<0.2$  s and error in location  $<1$  km. The dark cluster is related to the aftershocks of magnitude 4.5 of July 3. Cross-sections are indicated. Faults are shown as in Fig. 2. The epicentres of the largest earthquakes are shown.

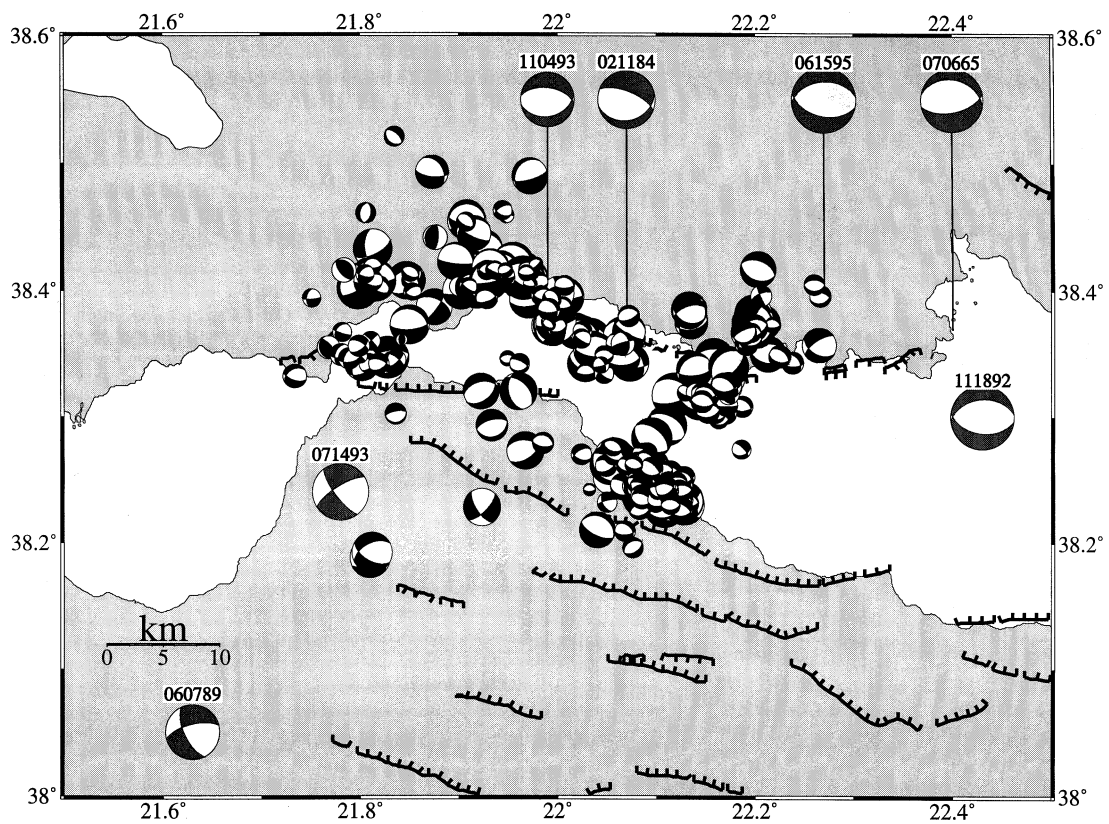


Figure 10. Map of the 377 focal mechanisms computed for July and August 1991 around Patras.

collected during July, giving a total of more than 4500 events. To confirm the interpretation deduced from the seismicity, we made further tests and selected the 750 events recorded by more than eight stations and located with an rms error of less than 0.2 s and an uncertainty of less than 1 km in epicentre and depth.

### Seismicity

The seismicity pattern (Fig. 9) is similar to that presented by Rigo *et al.* (1996). It is mostly restricted to the Gulf and most of the activity is observed beneath the northern side. One cluster is clearly associated with the magnitude  $M_l = 4.5$  event of July 3 located near Aigion (38.2°N, 22.1°E). The two other clusters described by Rigo *et al.* (1996) are not so obvious on our map, probably because our selection requires a minimum of eight stations, which slightly increases the magnitude threshold of the located events. The faults south of 38.2°N do not seem to be seismically active.

Cross-sections trending N–S across the Gulf show that seismicity is restricted to a depth of between 7 and 13 km (Fig. 11). The seismicity in the western cross-section AA' is restricted mostly between 8 and 11 km depth. As pointed out by Rigo *et al.* (1996), this seismicity distribution does not outline the geometry of the active faults at depth and some clusters could even be related to the Psathopyrgos or Helike

faults. Rigo *et al.* (1996) suggested that the seismicity dipping gently northwards might be associated with a low-angle normal fault or a detachment zone dipping at an angle of 15° but, as shown later, this is not consistent with the focal mechanisms. The eastern cross-section BB' is a little confused, due to the magnitude 4.5 aftershock cluster, but it is consistent with an almost subhorizontal extent of seismic events. On both sections, the microearthquakes are located at the same depth as the three strong events of 1965, 1992 and 1995, whose depths are well controlled by body wave modelling.

### Focal mechanisms

Focal mechanisms for August 1991 have already been presented by Rigo *et al.* (1996). A further 236 mechanisms for earthquakes in July have been added, making a total of 377 fault plane solutions (Fig. 11). The majority of the mechanisms correspond to E–W-striking faults with N–S extension. Most of the mechanisms show one plane dipping northwards at an angle of between 30° and 50° and therefore do not align with the shallow-dipping seismicity. A few strike-slip mechanisms, consistent with a N–S-trending T-axis, are, however, observed in the eastern part of the seismicity zone. The question remains whether the shallow-dipping seismicity is related to a shallow dipping décollement zone or to the brittle–ductile transition.

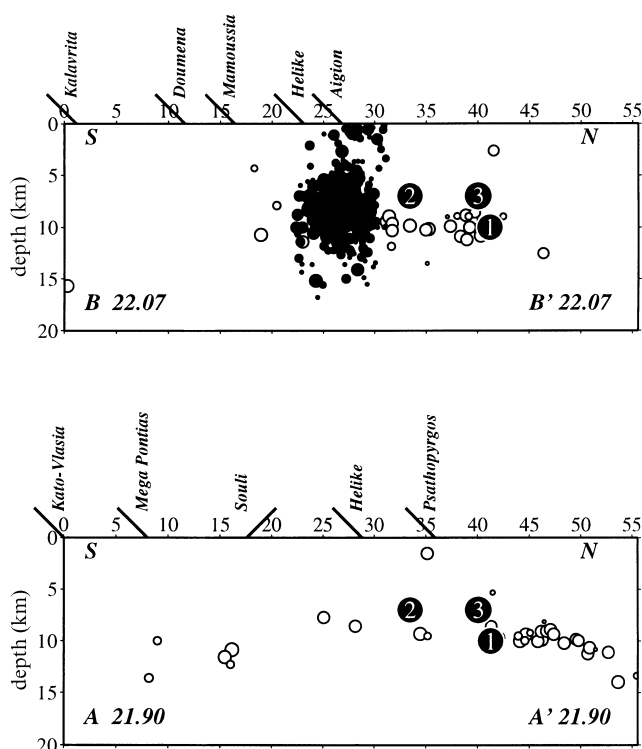


**Figure 11.** Cross-sections across the western Gulf of Corinth. The shallow north-dipping seismicity may be due either to a fault of listric shape or to the brittle–plastic transition. The dark cluster is related to the July 3, aftershocks. Fault traces are indicated and the largest earthquakes are shown. Numbers refer to the events of 1965, 1992 and 1995 with depths constrained by body wave modelling (Baker *et al.* 1997; Hatzfeld *et al.* 1996; Bernard *et al.* 1997).

### THE GALAXIDI EARTHQUAKE OF 1992 NOVEMBER 18

This earthquake of magnitude  $M_s = 5.9$  occurred on 1992 November 18, on the eastern side of the region studied during the summer of 1991. Body wave modelling of the main shock indicates a depth of 7.5 km and a mechanism showing normal faulting on an E–W-striking fault. There were very few aftershocks, located between 6 and 12 km depth, and not really discernible within the background seismicity. The dip of the inferred fault plane of the main shock is 30°N, which is consistent with the dip of the aftershock seismicity that is probably connected to the Helike fault. The small number of aftershocks (like the 1965 Eratini aftershocks located at the same place as the Galaxidi event) suggests that the Galaxidi event is related to an asperity located between the Helike fault and the Xylokaastro fault (Hatzfeld *et al.* 1996).

### THE PATRAS EARTHQUAKE OF 14 JULY 1993

This earthquake of magnitude  $M_s = 5.4$  occurred on the western side of the city of Patras and caused heavy damage. Two days after the main shock 10 portable seismological stations were installed around the epicentral area (Karakostas *et al.* 1994) and recorded about 250 aftershocks, 120 of which were recorded by more than 10 stations with an uncertainty of less than 3 km. The CMT solution of the main shock is a strike-slip mechanism, left lateral on a NNW–SSE-striking vertical plane (Figs 2 and 11). This is surprising in the general pattern of E–W-striking normal faults generally seen in the Gulf of Corinth. It is similar to another CMT solution located further

west (on 1989 June 7) and to microearthquake focal solutions computed by Hatzfeld *et al.* (1990). Aftershock fault plane solutions show both strike-slip faulting, similar to the main shock, for the shallowest events, and dip-slip solutions for the deepest events. A cross-section indicates only a slight deepening of the events towards the southeast, but does not give very much help in understanding the geometry of the main fault, which cannot be easily related to any surface fault (Rigo *et al.* 1996; Armijo *et al.* 1996).

## THE AIGION EARTHQUAKE OF 1995 JUNE 15

This earthquake of magnitude  $M_s = 6.2$  was the strongest event recorded in the Gulf of Corinth since the 1981 earthquake sequence. An extensive study by Bernard *et al.* (1997) describes the general characteristics of this earthquake. It occurred between the 1991 study area, where a cluster of activity was located, and the 1992 Galaxidi event. A study of the directivity, and the short-period hypocentre relocation suggest that the main shock is likely to have started at a depth of 10 km and propagated southwards towards the surface. The centroid depth, however, is 7.2 km, similar to the Galaxidi event. The mechanism (Figs 2 and 11) is a pure normal fault on an E–W-striking fault plane. The event occurred on the north-dipping plane at an angle of  $33^\circ$  and could well be related to the Helike fault given the uncertainties in main shock location and mechanism, or to a fault located offshore further north as proposed by Bernard *et al.* (1997). All the aftershocks were surprisingly located to the west of the main shock hypocentre at depths ranging from 5 to 9 km and were not located on a plane as defined by the main shock mechanism (Bernard *et al.* 1997).

## DISCUSSION

### Active faults and segmentation

The microseismicity experiments, like the few aftershock studies, show that seismicity is mostly restricted to the Gulf of Corinth. The faults that seem to be seismically active are mainly the north-dipping faults that bound the Gulf to the south. Seismicity is associated with the Psathopyrgos, Aigion, Helike and Xylokastro faults in the western and central parts of the Gulf, and to the Alepohori, Pisia, Psatha and Kaparelli faults in the eastern part of the Gulf. However, the Doumena, Souli, Mamoussa and Mega-Pontias faults, located further south, do not seem to be seismically active. The present deformation is therefore very localized within the Gulf of Corinth as also indicated by Quaternary tectonics (Armijo *et al.* 1996) and by geodetic observations that support a present-day deformation confined within the gulf (Clarke *et al.* 1997; Briole *et al.* 1999). This conclusion should be balanced by the results of another microseismicity experiment that surveyed the whole Peloponnese and located a few earthquakes south of the Gulf. However, these were of small magnitude and could be related to small-scale secondary faults (Hatzfeld *et al.* 1990).

Moreover, there is clearly no major seismicity related to the steep south-dipping faults that bound the Gulf of Corinth to the north, which may be interpreted as antithetic faults. Only the Kaparelli fault, and possibly the Delphi fault in 1970, is associated with seismicity, but the Eratini, Galaxidi and Antikira faults do not seem to be seismically active.

The earthquake potential of the faults in the Gulf of Corinth has been examined from a tectonic point of view. On the basis of fault segmentation (Jackson & White 1989; Roberts & Jackson 1991) it is suggested that the maximum magnitude expected on a single segment is not greater than  $M_w = 6.7$ , which is also the maximum magnitude estimated for historical events (Ambraseys & Jackson 1997; Papazachos & Papazachou 1997).

### Plastic–brittle transition

Seismicity is restricted to the brittle part of the crust, but the question remains whether a strong earthquake could modify the depth of the brittle–plastic transition (Sibson 1982) or whether the rupture due to excess strain could propagate within the lower crust (Boatwright 1985; Jackson & White 1989; Eyidogan & Jackson 1985). The brittle–ductile transition depth given by strong events or aftershocks could therefore be biased. Given that both background seismicity and aftershocks were recorded in the same place using the same techniques and the locations were determined with approximately the same uncertainties, the possibility of the plastic–brittle transition being modified by a strong earthquake was investigated. In the Gulf of Corinth, the depth of the microearthquakes seems to be the same before and after strong events, and the strong events seem to nucleate at the base of the brittle–ductile transition. This is true east of Corinth, comparing the 1993 experiment with the 1981 aftershocks, both of which range between 4 and 13 km. This is also true for the Galaxidi and Aigion aftershocks, which are located at the same depth (between 8 and 12 km) as the 1991 microearthquakes.

There is therefore no evidence in the aftershock sequence of a rupture propagation that could penetrate beneath the seismogenic layer for more than 2 km due to an increase in strain rate during the main shock. The only possibility of such a propagation is a dynamic effect seen only during the main shock itself.

### Faulting geometry

In the western Gulf of Corinth, the cut-off of the seismicity with depth is almost horizontal (Fig. 10), deepening gently from south to north, possibly suggesting a seismically active almost horizontal fault (Rigo *et al.* 1996). Moreover, precise relocation of a few small events within a cluster also supports the idea of shallow-dipping faulting (Rietbrock *et al.* 1996). On the other hand, most of the surface faults dip at about  $50^\circ$  N and all the fault planes of strong earthquakes dip between  $50^\circ$  and  $30^\circ$ . In the case of the 1995 Aigion event, it seems unlikely that the main shock was located on the prolongation of the surface faults dipping  $50^\circ$  N. On the other hand, a fault plane geometry dipping  $30^\circ$  N does not explain the morphology of the Gulf, assuming a flexural process alone (Bernard *et al.* 1997). Therefore, the relation between surface faulting and earthquake mechanism is not obvious.

If there is an almost horizontal décollement zone, the north-dipping fault planes of all mechanisms should align with the seismicity. The inferred north-dipping fault plane of the focal

mechanisms (both strong events and microearthquakes) was plotted (Fig. 12) on several sections across the Gulf using the Corinth 1981, Corinth 1993, Galaxidi 1992 and Patras 1991 observations. The dips of the microearthquake fault planes are

consistent with those of the strongest events obtained by body wave modelling and likely to be constrained within  $15^\circ$ . Around the eastern part of the Gulf, the dip is about  $45^\circ$  and supports the theory that the Kaparelli and Alephori faults are planar

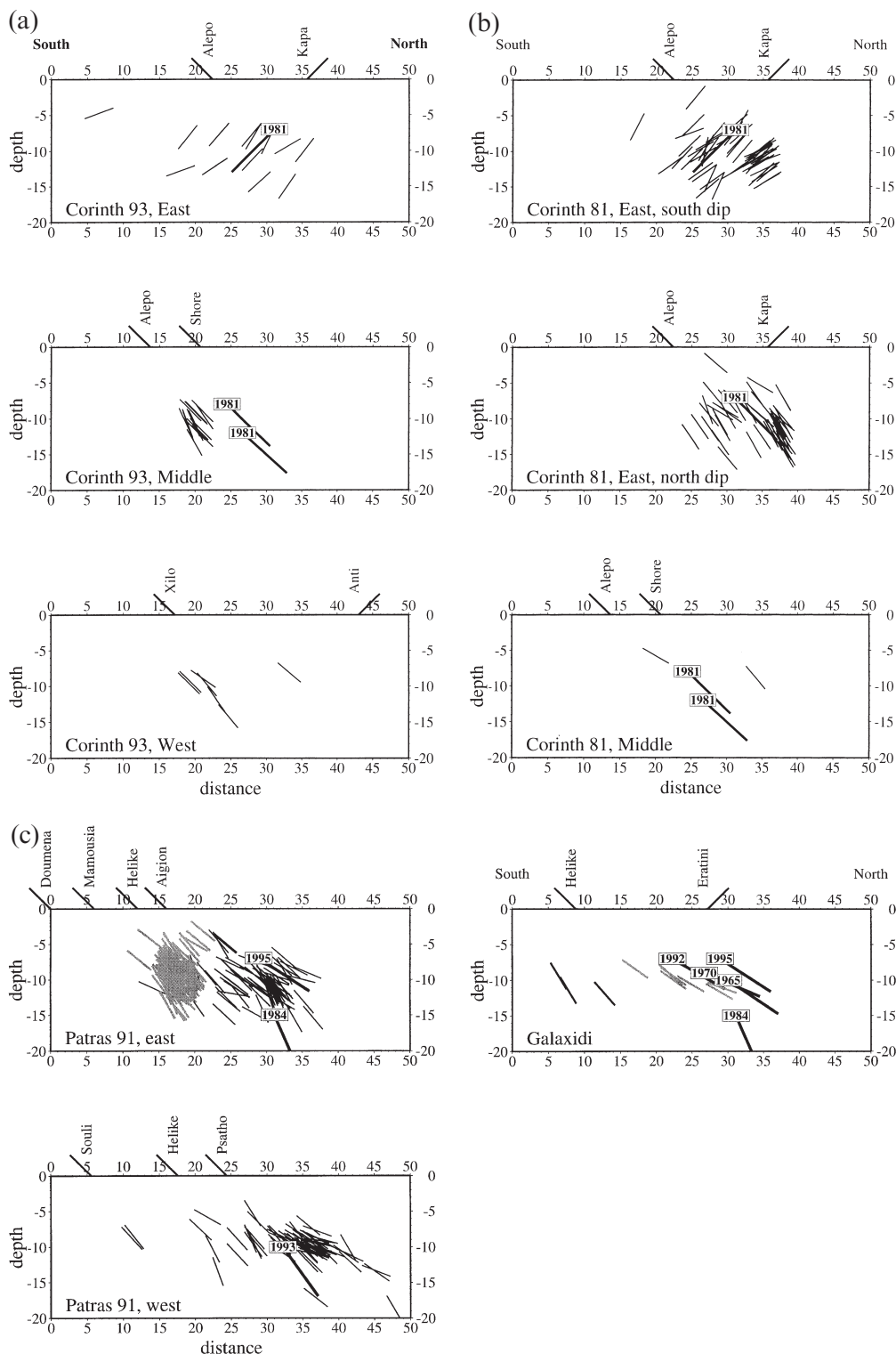


**Figure 12.** Cross-sections of the Gulf of Corinth. The figure shows the traces of the inferred fault planes on the cross-sections whose location are given in Fig. 2. Thick lines show the modelled mechanisms of Fig. 2, which are identified by their date in a box. The fault traces are shown. Grey lines refer to the main cluster during the 1991 experiment (Rigo *et al.* 1996) and to the Galaxidi aftershocks (Hatzfeld *et al.* 1996). Note that the dip of the fault plane is about  $45^\circ$  in the eastern Gulf of Corinth and about  $30^\circ$  in the western Gulf of Corinth around Patras.

and seismically active faults. This is true both for the 1981 aftershocks and for the 1993 microearthquakes. Further west, the fault planes of the Galaxidi aftershocks and Patras 1991 microearthquakes dip slightly more horizontally, between 40° and 20°N. The fault planes seem to align with the Helike fault at the surface.

This suggests that the background seismicity, which was previously associated with a north-dipping décollement (Rigo *et al.* 1996), does in fact mark the brittle–ductile transition. Microearthquake mechanisms, which are very similar to the strongest events, dip steeper than 15°, between 20° and 50°, and could represent small faults located at the base of the brittle crust. In the case of the Patras 1991 data, the microearthquake mechanisms may support the theory that the Helike fault dips 50°N at the surface but is not connected to the deeper faults that dip at 30°.

**Differences between west and east**

There are several marked differences between the eastern part of the Gulf near Corinth, and the western part near Patras (Fig. 13).

(1) The maximum depth of the seismicity is slightly different. In the westernmost part, the depth is restricted to 8–11 km, while in the east it ranges from 4 to 13 km. According to the accuracy of our locations, this could indicate that the brittle–ductile transition is slightly deeper in the eastern part of the Gulf. Again, this is true both for the background seismicity and for the aftershocks.

(2) Antithetic faults are active in the east but do not seem to be active in the west. In the east, the Kaparelli fault was

certainly active during the 1981 sequence (King *et al.* 1985), while there is no evidence that the Antikira, Eratini and Delphi faults were active during microseismicity experiments or the aftershock period.

(3) The extension rate is about  $15 \pm 2 \text{ mm yr}^{-1}$  in the west and about  $10 \pm 4 \text{ mm yr}^{-1}$  in the east (Clarke *et al.* 1997; Briole *et al.* 1999).

(4) The dips of the fault planes related to strong events are different for earthquakes located around Patras and around Corinth. To the west of the Gulf, the faults dip at a shallow angle of 30°N, such as the Aigion and Galaxidi events or the 1965 July 6 and 1970 April 8 earthquakes (Baker *et al.* 1997), assuming the north-dipping plane to be the active fault. To the east, they have a steeper dip (42°–45°) in the three events of 1981. This is not so obvious for the CMT solutions that were computed for two events (1993 November 4 and 1984 February 11), which may, however, be less accurate.

**Implications**

In summary, towards the western and narrower part of the Gulf of Corinth, around Patras, the present-day deformation rate is 50 per cent faster, the seismicity is slightly shallower, the fault planes dip at a shallower angle and antithetic faults are less extensive than in the eastern part of the Gulf, around Corinth.

The elastic model proposed by Armijo *et al.* (1996) for the Xylokaastro fault dipping 45°N seems to be able to reproduce the morphology of the eastern part of the Gulf. However, this model does not explain the western part of the Gulf because there are contradictions between the dip of the active fault, which is shallower than in the east, the rate of slip along the fault, which is greater assuming the present-day extension, and the topography. Moreover, recently formed normal faults should dip steeper than 45° in order to respect Coulomb failure values and this is not seen in the strong earthquakes. Therefore, the newly formed faults that dip at 30° (as in the western Gulf) have been explained either by high fluid pressure or by a non-vertical maximum compressive stress (Bernard *et al.* 1997).

An alternative possibility to explain the shallow-dipping active fault planes is that the 30° dipping faults are not newly formed in a flawless crust (as assumed by Coulomb failure criteria) but pre-existed and constitute a weakness zone. In this case, the angle between the fault and the principal stress is smaller and can reach values of 30° assuming a friction law on pre-existing faults that is only 30 per cent weaker than the coefficient of internal friction. Instead of assuming complex mechanisms involving fluids or principal stress rotations (which seems unlikely between the two ends of the Gulf), an alternative suggestion is that previous tectonics and inherited faults play a major role in the geometry of the active faults.

One possibility for obtaining faults dipping at 30° is therefore that the faults were originally created with a dip of 45° and rotated by 15° around a horizontal axis to a shallower dip.

**A speculative model**

The rotating domino model (e.g. Jackson & McKenzie 1983) is the simplest way to rotate faults (Fig. 13). The reason for the rotation of the active faults located in the western part of the Gulf of Corinth may be the present-day greater extension rate compared to the eastern part of the Gulf. In fact, a

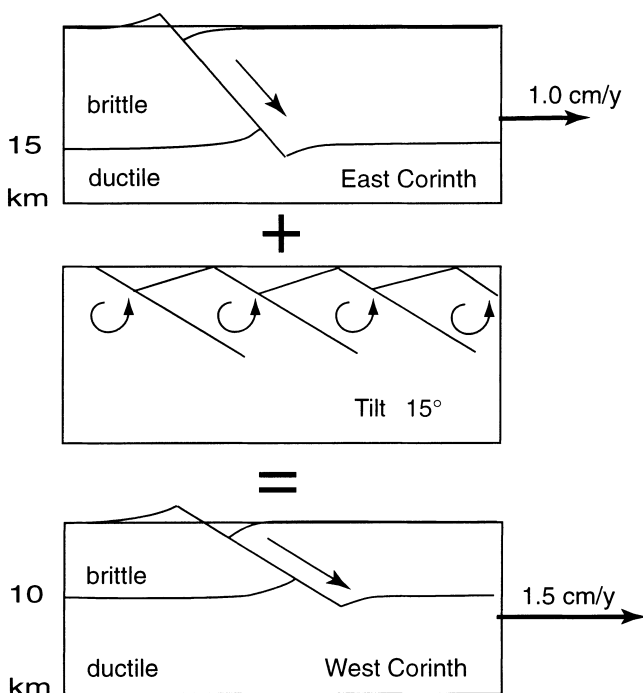


**Figure 13.** Differences between the eastern Gulf around Corinth and the western Gulf around Aigion. The faulting geometry in the western Gulf could be due to the rotation around a horizontal axis of a normal fault system dipping originally at 45° (as in the eastern Gulf) due to an increase in the extension rate.

rotation of the faults from  $45^\circ$  to  $30^\circ$  induces an extension factor of 1.4 (Jackson & McKenzie 1983). This difference in extension is consistent with the present-day 50 per cent increase in deformation rate measured by GPS between the western and eastern parts of Gulf (Briole *et al.* 1999).

A rotation around a horizontal axis of the active faults from  $45^\circ$  to  $30^\circ$  creates topographical landforms and induces extra slip along the fault. The extent of these topographical landforms and the amount of slip depend on the horizontal distance between faults. Assuming a horizontal distance of about 8 km, which is the average distance between the Aigion, Helike, Mamoussa, Doumena and Kalavrita faults, this gives an increase in topographical elevation of about 1.5 km (not taking into account the erosion), and an amount of slip due to rotation of about 3 km. These are reasonable values compared to the elevation of Quaternary sediments above the Psathopyrgos fault (700 m) and above the Xylokaastro fault (1700 m) and compared to the total slip of 11.5 km for the Xylokaastro fault assuming a pure elastic model (Armijo *et al.* 1996).

On the other hand, the brittle–ductile transition is likely to be due to a temperature profile and does not depend on the base of the rotating dominoes but only on the extension rate (Jackson & White 1989). A sudden stretching of 40 per cent will lead to a corresponding 40 per cent rise in the brittle–ductile transition (England & Jackson 1987), for instance from 15 km to 11 km (which is similar to the seismicity depth variation between the eastern and western parts of the Gulf of Corinth). This change will decay with a time constant related to diffusivity and block spacing.

The difference in the dip of the active faults between the western and eastern parts of the Gulf of Corinth is therefore possibly explained by the difference in the observed extension rate, which rotates by  $15^\circ$  pre-existing faults originally dipping at  $45^\circ$ .

Most of the geodynamical models for western Greece and the Peloponnese assume a clockwise rotation of western Greece and the Peloponnese (e.g. Le Pichon & Angelier 1979) consistent with post-Miocene palaeomagnetic measurements (Kissel & Laj 1988). However, Duermeijer *et al.* (1999) dated the rotation of Zakynthos island precisely and showed that all the  $21.6^\circ$  clockwise rotation occurred since 0.77 Ma. This rotation is slightly larger than the Pleistocene rotation observed for the Peloponnese (Kissel & Laj 1988).

First, the greater rotation of the Ionian islands compared to the Peloponnese induces a greater extension rate across the western Gulf of Corinth compared to the eastern Gulf as evidenced by geodesy (Clarke *et al.* 1997). This extension is even greater toward the Ionian islands (Kahle *et al.* 1995). Second, the timing of the Zakynthos rotation is synchronous with an increase in the tectonic activity over all the Aegean (Mercier *et al.* 1989), with the increase in extension observed for the Gulf of Corinth (Armijo *et al.* 1996), with a westward migration of the rifting within the Gulf (Doutsos & Poulimenos 1992) and with a northward migration of the surface faults in the westernmost Gulf (Sorel 1999). This increase in activity is especially clear in the Ionian islands and western Greece (e.g. Sorel 1989).

A possible scenario is that the Gulf of Corinth started to open in the upper Pliocene. In the late Pleistocene, a change occurred in the deformation of the Aegean due to several possible causes probably located at the edge (e.g. boundary

conditions, subduction) of the Aegean as evidenced by the recent rotation of Zakynthos. This change reorganized slightly the deformation field in the Aegean and modified the extensional processes affecting the Gulf of Corinth. Because of the increase in the stretching of the westernmost Gulf, it raised the brittle–ductile transition and rotated the faults inherited from the Pliocene in the western part of the Gulf around a horizontal axis.

## CONCLUSIONS

The results of a detailed microseismicity survey conducted at the eastern end of the Gulf of Corinth in 1993 are consistent with a reassessment of the 1981 aftershock sequence. The seismicity ranges between 4 and 13 km depth and affects both the north-dipping faults of Pisia and Alepohori and the antithetic south-dipping fault of Kaparelli. Mechanisms are consistent with N–S extension on E–W-trending planes dipping at  $45^\circ$  both northwards and southwards. There is no evidence of any connection with a low-angle fault zone dipping northwards at depth.

On the other hand, observations conducted in the western Gulf of Corinth suggest that the seismicity is restricted in the westernmost part between 8 and 11 km and dips at a very low angle to the north. Active fault planes dip at angles of  $20^\circ$  to  $50^\circ$  for the microearthquakes and about  $30^\circ$  for the strongest events.

Therefore, at both ends of the Gulf, the seismically active faults dip steeper than  $10^\circ$ – $15^\circ$  and are not related to an almost horizontal active fault that could be inferred from the cut-off of the seismicity at depth. This cut-off seems instead to represent the seismic–aseismic transition and is not consistent with a possible décollement.

A model of rotating faults around a horizontal axis (the domino model) resulting from the recent greater degree of extension in the western Gulf could explain the change from faults dipping originally at  $45^\circ$  to faults dipping at  $30^\circ$ . This model is consistent with the topography and the rise in the brittle–ductile transition.

## ACKNOWLEDGMENTS

The Corinth 1993 experiment was supported by the EC EPOC-CT91–0043 contract. The authors are deeply grateful to J. Jackson and G. King for providing their original records of the 1981 aftershock sequence. H. Lyon-Caen participated in the experiments and in data processing. The authors also wish to thank G. Bock, J. Jackson, P. Molnar, A. Rigo and T. Taymaz for their helpful comments on the manuscript.

## REFERENCES

- Abercrombie, R.E., Main, I.C., Douglas, A. & Burton, P.W., 1995. The nucleation and rupture process of the 1981 Gulf of Corinth earthquakes from deconvolved broad-band data, *Geophys. J. Int.*, **120**, 393–405.
- Abers, G.A., Mutter, C.Z. & Fang, J., 1997. Shallow dips of normal faults during rapid extension: earthquakes in the Woodlark–D'Entrecasteaux rift system, Papua New Guinea, *J. geophys. Res.*, **102**, 15 301–15 317.

- Allmendiger, R.W., Sharp, J.W., Von Tish, D., Serpa, L., Brown, L., Kaufman, S., Oliver, J. & Smith, R.B., 1983. Cenozoic and Mesozoic structure of the Eastern Basin and Range Province Utah, from COCORP seismic-reflection data, *Geology*, **11**, 532–536.
- Ambraseys, N. & Jackson, J., 1990. Seismicity and associated strain of Central Greece between 1890 and 1988, *Geophys. J. Int.*, **101**, 663–708.
- Ambraseys, N.N. & Jackson, J.A., 1997. Seismicity and strain in the Gulf of Corinth (Greece) since 1694, *J. Earthq. Eng.*, **1**, 433–474.
- Armijo, R., Meyer, B., King, G.C.P., Rigo, A. & Papanastassiou, D., 1996. Quaternary evolution of the Corinth Rift and its implications for the late Cenozoic evolution of the Aegean, *Geophys. J. Int.*, **126**, 11–53.
- Baker, C., Hatzfeld, D., Lyon-Caen, H., Papadimitriou, E. & Rigo, A., 1997. Earthquake mechanisms of the Adriatic sea and western Greece, *Geophys. J. Int.*, **131**, 559–594.
- Bernard, P. *et al.*, 1997. A low angle normal fault earthquake: the Ms = 6.2, June 1995 Aigion earthquake (Greece), *J. Seism.*, **1**, 131–150.
- Bezzeghoud, M., Deschamps, A. & Madariaga, R., 1986. Broad-band modelling of the Corinth, Greece earthquakes of February and March 1981, *Ann. Geophys.*, **4**, 295–304.
- Billiris, H. *et al.*, 1991. Geodetic determination of the strain of Greece in the interval 1900–88, *Nature*, **350**, 124–129.
- Boatwright, J., 1985. Characteristics of the aftershock sequence of the Borah Peak, Idaho, earthquake determined from digital recordings of the events, *Bull. seism. Soc. Am.*, **75**, 1265–1284.
- Braunmiller, J. & Nabelek, J., 1996. Geometry of continental normal faults: seismological constraints, *J. geophys. Res.*, **101**, 3045–3052.
- Briole, P. *et al.*, 1999. Active deformation of the Gulf of Korinthos, Greece: results from repeated GPS surveys between 1990 and 1995, *Geophys. J. Int.*, in press.
- Brooks, M. & Ferentinos, G., 1984. Tectonics and sedimentation in the Gulf of Corinth and the Zante and Cephalonia channels, western Greece, *Tectonophysics*, **101**, 25–54.
- Clarke, P.J. *et al.*, 1997. Geodetic estimate of seismic hazard in the Gulf of Korinthos, *Geophys. Res. Lett.*, **24**, 1303–1306.
- Collier, R.E., 1990. Eustatic and tectonic controls upon Quaternary coastal sedimentation in the Corinth Basin, Greece, *J. geol. Soc. Lond.*, **147**, 301–314.
- Davies, R., England, P., Billiris, H., Paradissis, D. & Veis, G., 1997. A comparison between the geodetic and seismic strain of Greece in the interval 1892–1992, *J. geophys. Res.*, in press.
- DeMets, C., Gordon, R.G., Argus, D.F. & Stein, S., 1990. Current plate motions, *Geophys. J. Int.*, **101**, 425–478.
- Doutsos, T. & Piper, D.J., 1990. Listric faulting, sedimentation, and morphological evolution of the Quaternary eastern Corinth rift, Greece: first stages of continental rifting, *Geol. Soc. Am. Bull.*, **102**, 812–829.
- Doutsos, T. & Poulimenos, G., 1992. Geometry and kinematics of active faults and their seismotectonic significance in the western Corinth-Patras rift (Greece), *J. struct. Geol.*, **14**, 689–699.
- Duermeijer, C.E., Krijgsman, W., Langereis, C.G., Meulenkaamp, J.E., Triantaphyllou, M.V. & Zachariasse, W.J., 1999. A Late Pleistocene clockwise rotation phase of Zakynthos (Greece) and implications for the evolution of the western Aegean arc, *Earth planet. Sci. Lett.*, **173**, 315–331.
- England, P. & Jackson, J., 1987. Migration of the seismic-aseismic transition during uniform and nonuniform extension of the continental lithosphere, *Geology*, **15**, 291–294.
- Eyidogan, H. & Jackson, J., 1985. A seismological study of normal faulting in the Demirci, Alashir and Gediz earthquakes of 1969–70 in western Turkey: implications for the nature and geometry of deformation in continental crust, *Geophys. J. R. astr. Soc.*, **81**, 569–607.
- Hatzfeld, D., Pedotti, G., Hatzidimitriou, P. & Makropoulos, K., 1990. The strain pattern in the western Hellenic arc deduced from a microearthquake survey, *Geophys. J. Int.*, **101**, 181–202.
- Hatzfeld, D. *et al.*, 1996. The Galaxidi earthquake sequence of November 18, 1992: a possible geometrical barrier within the normal fault system of the Gulf of Corinth (Greece), *Bull. seism. Soc. Am.*, **86**, 1987–1991.
- Hubert, A., King, G., Armijo, R., Meyer, B. & Papanastassiou, D., 1996. Fault re-activation, stress interaction and rupture propagation of the 1981 Corinth earthquake sequence, *Earth planet. Sci. Lett.*, **142**, 573–585.
- Jackson, J.A., 1987. Active normal faulting and crustal extension, in *Continental Extensional Tectonics*, eds Coward, M.P., Dewey, J.F. & Hancock, P.L., *Geol. Soc. Lond. Spec. Publ.*, **28**, 3–17.
- Jackson, J.A., 1994. The Aegean deformation, *Ann. Rev. Geophys.*, **22**, 239–272.
- Jackson, J.A. & McKenzie, D.P., 1983. The geometrical evolution of normal fault systems, *J. struct. Geol.*, **5**, 471–482.
- Jackson, J.A. & White, N.J., 1989. Normal faulting in the upper continental crust: observations from regions of active extension, *J. struct. Geol.*, **11**, 15–36.
- Jackson, J.A., Gagnepain, J., Houseman, G., King, G.C.P., Papadimitriou, P., Soufleris, C. & Virieux, J., 1982. Seismicity, normal faulting, and the geomorphological development of the Gulf of Corinth (Greece): the Corinth earthquakes of February and March 1981, *Earth planet. Sci. Lett.*, **57**, 377–397.
- Kahle, H.-G., Müller, M.V., Geiger, A., Danuser, G., Mueller, S., Veis, G., Billiris, H. & Paradissis, D., 1995. The strain field in NW Greece and the Ionian islands: results inferred from GPS measurements, *Tectonophysics*, **249**, 41–52.
- Karakostas, B. *et al.*, 1994. The aftershock sequence and focal properties of the July, 1993 (Ms = 5.4) Patras earthquake, *Bull. geol. Soc. Greece*, **XXX/5**, 167–174.
- King, G.C.P. *et al.*, 1985. The evolution of the Gulf of Corinth (Greece): an aftershock study of the 1981 earthquakes, *Geophys. J. R. astr. Soc.*, **80**, 677–693.
- Kissel, C. & Laj, C., 1988. The tertiary geodynamical evolution of the Aegean arc; a paleomagnetic reconstruction, *Tectonophysics*, **146**, 183–201.
- Leeder, M.R., Seger, M.J. & Stark, C.P., 1991. Sedimentation and tectonic geomorphology adjacent to major active and inactive normal faults, southern Greece, *J. geol. Soc. Lond.*, **148**, 331–343.
- Le Pichon, X. & Angelier, J., 1979. The Hellenic arc and trench system: a key to the neotectonic evolution of the Eastern Mediterranean region, *Tectonophysics*, **60**, 1–42.
- Le Pichon, X., Chamot-Rooke, N., Lallemand, S., Noomen, R. & Veis, G., 1995. Geodetic determination of the kinematics of Central Greece with respect to Europe: implications for eastern Mediterranean tectonics, *J. geophys. Res.*, **100**, 12 675–12 690.
- Mariolakis, I. & Stiros, S.C., 1987. Quaternary deformation of the Isthmus and Gulf of Corinthos (Greece), *Geology*, **15**, 225–228.
- McKenzie, D.P., 1978. Active tectonics of the Alpine-Himalayan belt: the Aegean Sea and surrounding regions, *Geophys. J. R. astr. Soc.*, **55**, 217–254.
- Mercier, J.L., Carey, E., Philip, H. & Sorel, D., 1976. La néotectonique plio-quaternaire de l'arc égéen externe et de la mer Egée et ses relations avec la sismicité, *Bull. Soc. géol. Fr.*, **7**, 355–372.
- Mercier, J.L., Sorel, D., Vergely, P. & Simeakis, K., 1989. Extensional tectonic regimes in the Aegean basins during the Cenozoic, *Basin Res.*, **2**, 49–71.
- Papazachos, B. & Papazachou, K., 1997. *Earthquakes in Greece*, Ekdoseis Ziti, Thessaloniki.
- Poulimenos, G., Albers, G. & Doutsos, T., 1989. Neotectonic evolution of the Central Section of the Corinth Graben, *Z. dt. geol. Ges.*, **140**, 173–182.
- Reilinger, R., McClusky, S.C., Oral, M.B., King, R.W. & Toksoz, M.N., 1997. Global Positioning System measurements of present-day crustal movements in the Arabia-Africa-Eurasia plate collision zone, *J. geophys. Res.*, **102**, 9983–9999.
- Rietbrock, A., Tiberi, C., Scherbaum, F. & Lyon-Caen, H., 1996. Seismic slip on a low angle normal fault in the Gulf of Corinth:

- evidence from high-resolution cluster analysis of microearthquakes, *Geophys. Res. Lett.*, **23**, 1817–1820.
- Rigo, A., Lyon-Caen, H., Armijo, R., Deschamps, A., Hatzfeld, D., Makropoulos, K., Papadimitriou, P. & Kassaras, I., 1996. A micro-seismic study in the western part of the Gulf of Corinth (Greece): implications for large-scale normal faulting mechanisms, *Geophys. J. Int.*, **126**, 663–688.
- Roberts, S. & Jackson, J.A., 1991. Active normal faulting in Central Greece: and overview, in *The Geometry of Normal Faults*, eds Roberts, A.M., Yielding, G. & Freeman, B., *Geol. Soc., Lond. Spec. Publ.*, **56**, 125–142.
- Roberts, G., Gawthorpe, R. & Stewart, I., 1993. Surface faulting within active normal fault zones: examples from the Gulf of Corinth fault system, Central Greece, *Z. Geomorph. N.F.*, **94**, 303–328.
- Sibson, R.H., 1982. Fault zone models, heat flow, and the depth distribution of earthquakes in the continental crust of the United States, *Bull. seism. Soc. Am.*, **72**, 151–163.
- Sorel, D., 1989. L'évolution structurale de la Grèce nor-occidentale depuis le Miocène, dans le cadre géodynamique de l'arc égéen, *Thèse de Doctorat d'Etat*, Université de Paris-Sud.
- Sorel, D., 1999. A Pleistocene and still-active detachment fault and the origin of the Corinth-Patras rift (Greece), *Geology*, in press.
- Taymaz, T., Jackson, J.A. & McKenzie, D., 1991. Active tectonics of the north and Central Aegean Sea, *Geophys. J. Int.*, **106**, 433–490.
- Wernicke, B., 1985. Uniform sense simple shear of the continental lithosphere, *Can J. Earth Sci.*, **22**, 108–125.
- Wernicke, B., 1995. Low-angle normal faults and seismicity: a review, *J. geophys. Res.*, **100**, 20 159–20 174.

## APPENDIX A: FOCAL MECHANISMS

Table A1. Parameters of the focal mechanisms computed for Corinth 1993 and Corinth 1981.

Corinth 93, focal mechanisms														
N°	Date & Time		Lat °N	Long °E	Z km	Mag	Plan1		Plan2		P Axis		T Axis	
							Az	Pl	Az	Pl	Az	Pl	Az	Pl
16	930718	11:42	38.21	23.31	8.3	1.9	235	60	49	30	151	74	323	14
29	930719	20:39	38.13	23.18	10.0	1.9	250	80	350	45	199	38	307	21
85	930726	18:48	38.14	23.17	10.6	1.8	300	70	35	76	258	23	166	4
139	930731	5:38	38.16	23.23	6.2	2.2	40	49	160	59	15	54	278	5
165	930802	10:15	38.10	22.73	10.1	2.2	250	54	130	54	100	54	9	0
189	930804	8:39	38.11	22.87	12.6	2.0	240	49	60	40	149	85	330	4
250	930810	11: 8	38.07	23.01	11.5	2.4	240	60	49	30	163	74	326	14
284	930812	6:33	38.07	22.85	7.8	1.7	250	35	75	55	356	79	162	10
290	930812	11:23	38.18	23.27	6.7	.4	250	40	15	64	240	58	127	13
297	930812	14:12	38.08	22.78	8.2	1.5	295	49	99	40	257	81	18	4
301	930812	17:55	38.08	23.18	12.1	.6	290	70	109	20	199	65	19	24
309	930812	20:48	38.16	23.14	9.7	.8	240	44	40	46	234	79	139	0
333	930813	8:22	38.08	22.92	11.0	3.6	219	44	60	46	45	79	140	0
353	930813	15: 2	38.08	22.91	7.4	1.4	260	44	60	46	254	79	159	0
359	930813	20: 3	38.08	23.29	6.4	.4	219	40	60	51	20	78	141	5
382	930815	7:44	38.18	23.24	13.0	1.1	260	54	40	42	225	68	332	6
400	930816	5:41	38.20	23.17	13.0	1.7	280	70	24	54	237	40	335	9
403	930816	9:34	38.07	22.92	10.0	2.3	219	44	60	46	45	79	140	0
404	930816	9:41	38.07	22.92	7.8	1.4	240	44	89	49	67	74	165	2
405	930816	9:43	38.07	22.93	10.0	3.0	219	44	60	46	45	79	140	0
408	930816	18:16	38.06	22.92	7.4	1.4	219	44	70	49	47	74	145	2
413	930816	19:49	38.07	22.91	7.6	1.5	219	44	60	46	45	79	140	0
464	930818	20:47	38.06	22.90	8.1	2.3	219	44	80	52	50	68	151	4
466	930818	21: 9	38.12	23.31	6.2	.2	260	44	49	49	252	74	154	2
475	930819	1: 3	38.21	23.16	13.3	1.1	230	35	40	55	288	78	134	10
484	930819	5:24	38.06	22.91	8.6	1.7	300	65	89	28	235	67	19	18
525	930820	0:41	38.07	22.93	9.3	1.5	310	65	89	31	253	64	25	17
531	930820	2:28	38.07	22.93	8.7	1.0	329	65	120	28	265	67	49	18
541	930820	8:31	38.08	22.92	8.0	1.2	310	54	70	54	279	54	10	0
557	930820	19:44	38.18	22.77	6.8	1.5	199	40	89	73	39	47	152	20
574	930821	8: 1	38.23	23.26	8.3	.6	250	44	30	52	239	68	138	4
602	930822	8:52	38.06	22.92	8.7	1.5	310	70	89	25	244	61	27	23
645	930823	22:39	38.06	22.93	9.1	1.5	310	70	89	25	244	61	27	23

Table A1. (Continued.)

Corinth 81, focal mechanisms														
N°	Date & Time		Lat °N	Long °E	Z km	Mag	Plan1		Plan2		P Axis		T Axis	
							Az	Pl	Az	Pl	Az	Pl	Az	Pl
25	810308	4:18	38.15	23.12	8.7		250.0	60.0	80.0	30.4	146.6	74.5	343.7	14.9
26	810308	4:31	38.15	23.12	7.8		40.0	60.0	220.0	30.0	310.0	75.0	130.0	15.0
33	810308	14:17	38.23	23.25	5.2		240.0	60.0	350.0	59.4	204.7	45.6	295.1	.4
37	810308	18:25	38.17	23.21	6.0		210.0	40.0	40.0	50.4	349.0	82.8	125.5	5.2
62	810309	19:53	38.14	23.12	4.9		220.0	50.0	70.0	44.1	65.2	74.2	324.3	3.1
64	810309	21:22	38.17	23.16	6.7		230.0	50.0	60.0	40.4	98.5	83.1	324.6	4.8
73	810310	3:49	38.14	23.11	9.7	3.4	240.0	55.0	15.0	44.7	207.1	65.2	309.3	5.6
74	810310	4:9	38.12	23.11	9.4	3.0	250.0	55.0	20.0	47.4	218.5	62.1	316.4	4.2
90	810310	19:7	38.19	23.25	4.8		230.0	55.0	80.0	39.0	91.1	72.8	333.0	8.3
123	810312	11:15	38.20	23.24	6.2	2.5	230.0	50.0	30.0	41.8	198.4	79.1	310.7	4.2
127	810312	15:58	38.14	23.10	7.8		220.0	50.0	70.0	44.1	65.2	74.2	324.3	3.1
135	810313	0:31	38.23	23.26	9.3		230.0	60.0	90.0	37.0	96.3	66.7	336.3	12.2
142	810313	12:50	38.23	23.26	8.4		230.0	60.0	40.0	30.4	153.4	74.5	316.3	14.9
155	810314	2:33	38.23	23.25	8.9		240.0	60.0	60.0	30.0	150.0	75.0	330.0	15.0
164	810314	11:52	38.22	23.25	8.5		230.0	50.0	50.0	40.0	140.0	85.0	320.0	5.0
172	810314	19:23	38.22	23.24	10.8		230.0	60.0	50.0	30.0	140.0	75.0	320.0	15.0
175	810314	21:24	38.22	23.26	10.1		230.0	60.0	40.0	30.4	153.4	74.5	316.3	14.9
177	810314	23:55	38.22	23.26	9.2		230.0	60.0	70.0	31.6	114.4	72.9	327.5	14.4
178	810315	0:40	38.23	23.25	9.7		230.0	60.0	50.0	30.0	140.0	75.0	320.0	15.0
182	810315	7:0	38.23	23.26	9.7		230.0	60.0	50.0	30.0	140.0	75.0	320.0	15.0
188	810315	12:47	38.20	23.20	4.3		240.0	30.0	60.0	60.0	330.0	75.0	150.0	15.0
198	810316	0:11	38.14	23.16	.9		330.0	40.0	150.0	50.0	60.0	85.0	240.0	5.0
202	810316	3:26	38.22	23.25	10.4		230.0	60.0	50.0	30.0	140.0	75.0	320.0	15.0
205	810316	5:23	38.22	23.25	10.1		230.0	60.0	110.0	49.1	86.7	54.7	347.8	6.3
208	810316	6:18	38.23	23.25	8.1	2.9	245.0	50.0	30.0	45.7	221.3	71.5	318.1	2.3
209	810316	10:32	38.23	23.25	11.7		210.0	50.0	50.0	41.8	61.6	79.1	309.3	4.2
210	810316	10:37	38.23	23.25	12.1		210.0	50.0	50.0	41.8	61.6	79.1	309.3	4.2
212	810316	16:31	38.14	23.12	9.4		260.0	70.0	.0	64.5	218.6	33.1	311.0	3.6
213	810316	17:37	38.14	23.18	6.8		350.0	70.0	170.0	20.0	260.0	65.0	80.0	25.0
219	810317	0:32	38.14	23.13	10.0		260.0	70.0	.0	64.5	218.6	33.1	311.0	3.6
221	810317	2:2	38.16	23.13	7.9		270.0	70.0	10.0	64.5	228.6	33.1	321.0	3.6
222	810317	2:12	38.23	23.27	12.1		230.0	60.0	30.0	31.6	165.6	72.9	312.5	14.4
230	810317	10:50	38.24	23.25	12.9		230.0	60.0	30.0	31.6	165.6	72.9	312.5	14.4
233	810317	14:6	38.16	23.22	9.5		230.0	60.0	50.0	30.0	140.0	75.0	320.0	15.0
238	810317	22:24	38.24	23.24	13.2		240.0	60.0	60.0	30.0	150.0	75.0	330.0	15.0
241	810317	23:8	38.16	23.22	7.8		230.0	60.0	50.0	30.0	140.0	75.0	320.0	15.0
249	810318	6:43	38.23	23.25	10.5		240.0	60.0	50.0	30.4	163.4	74.5	326.3	14.9
255	810318	10:29	38.20	23.08	7.2		190.0	50.0	50.0	47.6	32.9	68.6	299.6	1.3
267	810319	9:55	38.06	23.04	4.8	3.0	315.0	30.0	160.0	62.4	96.0	70.1	241.0	16.5
273	810320	1:24	38.24	23.25	11.6	2.7	245.0	55.0	30.0	40.5	207.4	70.6	319.6	7.6
275	810320	5:21	38.19	23.20	11.8	2.7	230.0	60.0	50.0	30.0	140.0	75.0	320.0	15.0
280	810320	11:50	38.23	23.26	9.0	2.8	240.0	40.0	60.0	50.0	330.0	85.0	150.0	5.0
281	810320	14:4	38.15	23.27	11.6	3.0	340.0	55.0	150.0	35.4	272.0	79.1	65.9	9.8
286	810321	1:58	38.19	23.23	7.0	3.1	230.0	60.0	50.0	30.0	140.0	75.0	320.0	15.0
287	810321	2:46	38.20	23.24	10.8	2.9	340.0	55.0	160.0	35.0	250.0	80.0	70.0	10.0
289	810321	8:45	38.19	23.24	7.6	2.9	240.0	50.0	60.0	40.0	150.0	85.0	330.0	5.0
291	810321	13:55	38.16	23.13	13.9	3.1	240.0	50.0	60.0	40.0	150.0	85.0	330.0	5.0
293	810322	12:18	38.13	23.13	8.9	3.0	220.0	50.0	40.0	40.0	130.0	85.0	310.0	5.0
296	810322	16:28	38.23	23.25	11.7	2.9	245.0	65.0	55.0	25.3	163.7	69.7	331.8	19.9
301	810323	13:13	38.16	23.22	8.1	3.0	225.0	35.0	45.0	55.0	315.0	80.0	135.0	10.0
318	810324	21:51	38.17	23.09	13.0	2.6	140.0	35.0	10.0	65.8	319.0	60.4	81.1	16.8
324	810325	11:6	38.24	23.25	10.4	3.1	260.0	70.0	70.0	20.3	175.7	64.8	347.3	24.9
328	810326	4:23	38.16	23.09	11.9	2.8	140.0	35.0	10.0	65.8	319.0	60.4	81.1	16.8
330	810326	7:59	38.23	23.25	9.3	3.0	215.0	70.0	60.0	21.9	110.3	63.9	312.0	24.5
332	810326	16:40	38.10	23.03	10.3	3.7	145.0	75.0	40.0	46.0	13.3	42.4	266.1	18.0
333	810326	23:53	38.14	23.14	8.1	3.2	210.0	30.0	100.0	78.8	40.1	48.5	167.8	28.4
334	810327	14:59	38.20	23.25	8.5	3.0	140.0	40.0	330.0	50.4	279.0	82.8	55.5	5.2
336	810328	8:50	38.16	23.11	5.9	3.0	230.0	50.0	360.0	52.5	207.2	62.2	114.5	1.4
338	810328	20:40	38.19	23.25	5.9	2.9	150.0	45.0	10.0	52.5	341.0	68.4	81.2	4.0
340	810329	0:36	38.11	23.22	10.8	2.7	110.0	35.0	300.0	55.4	231.1	78.7	25.9	10.2

Downloaded from https://academic.oup.com/gji/article/141/2/438/648275 by guest on 11 March 2022

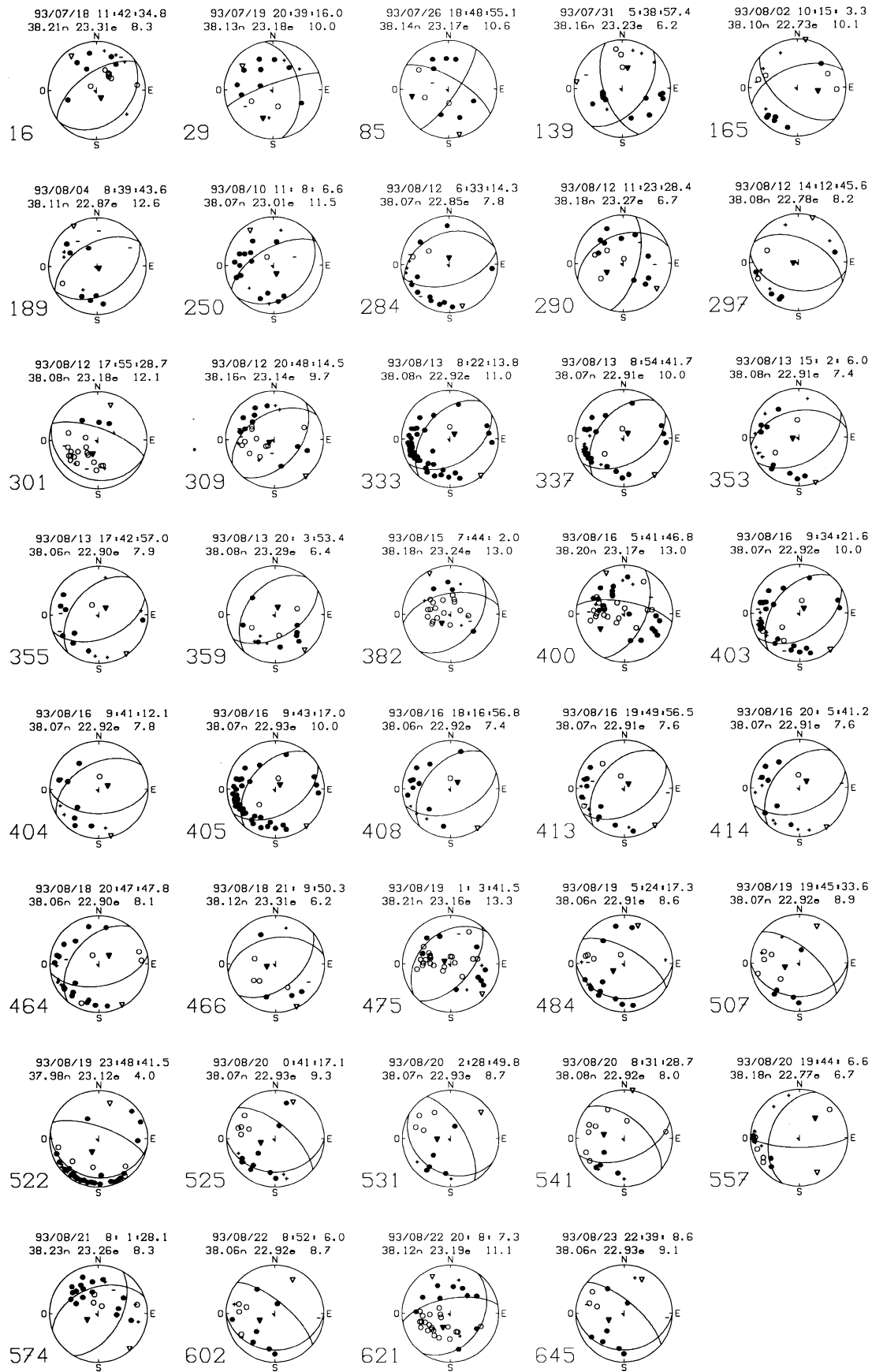


Figure A1. Lower hemisphere of focal spheres. Solid and open symbols are reliable compressional and dilatational first motions; + and - are uncertain.

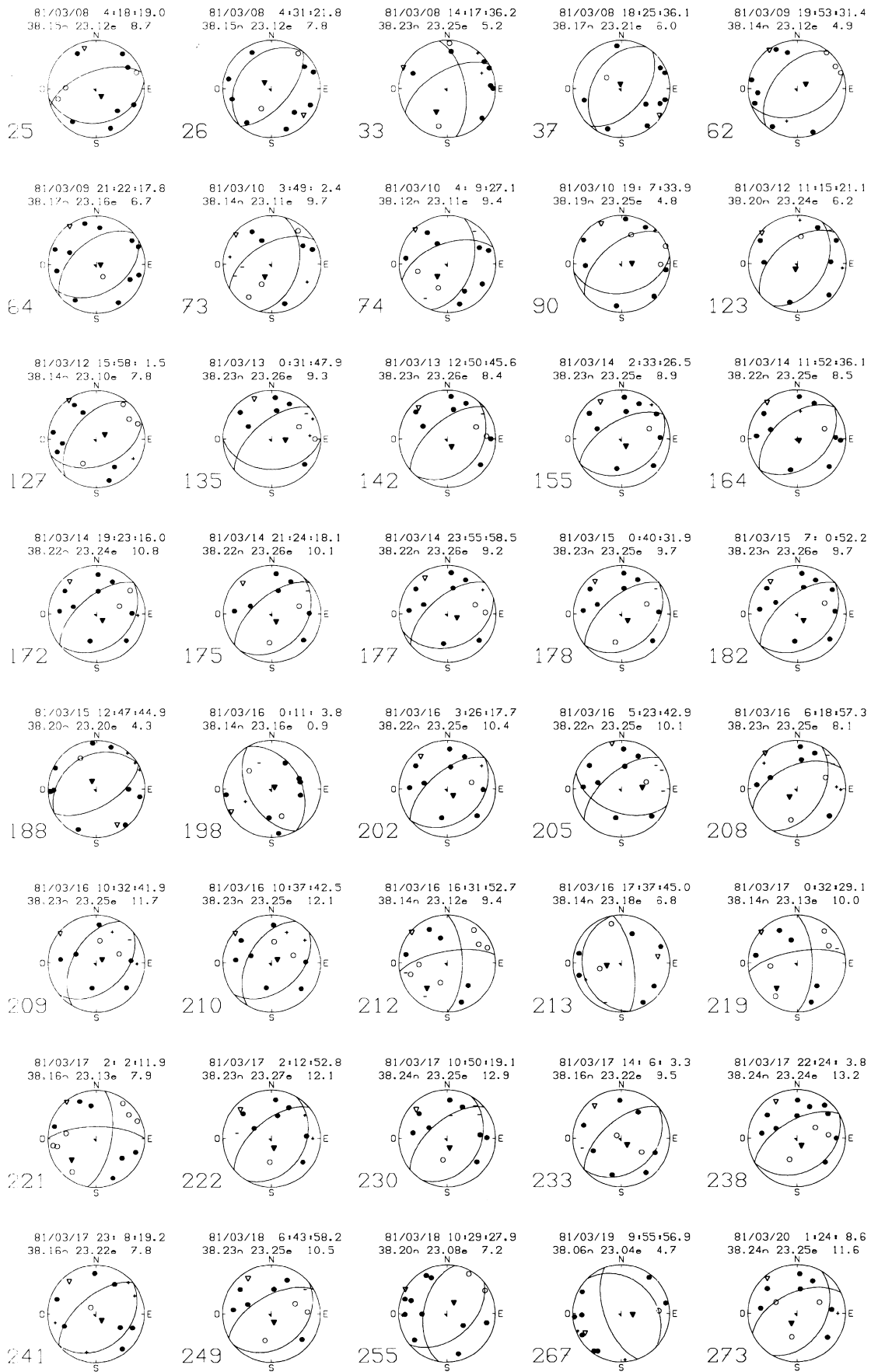


Figure A1. (Continued.)

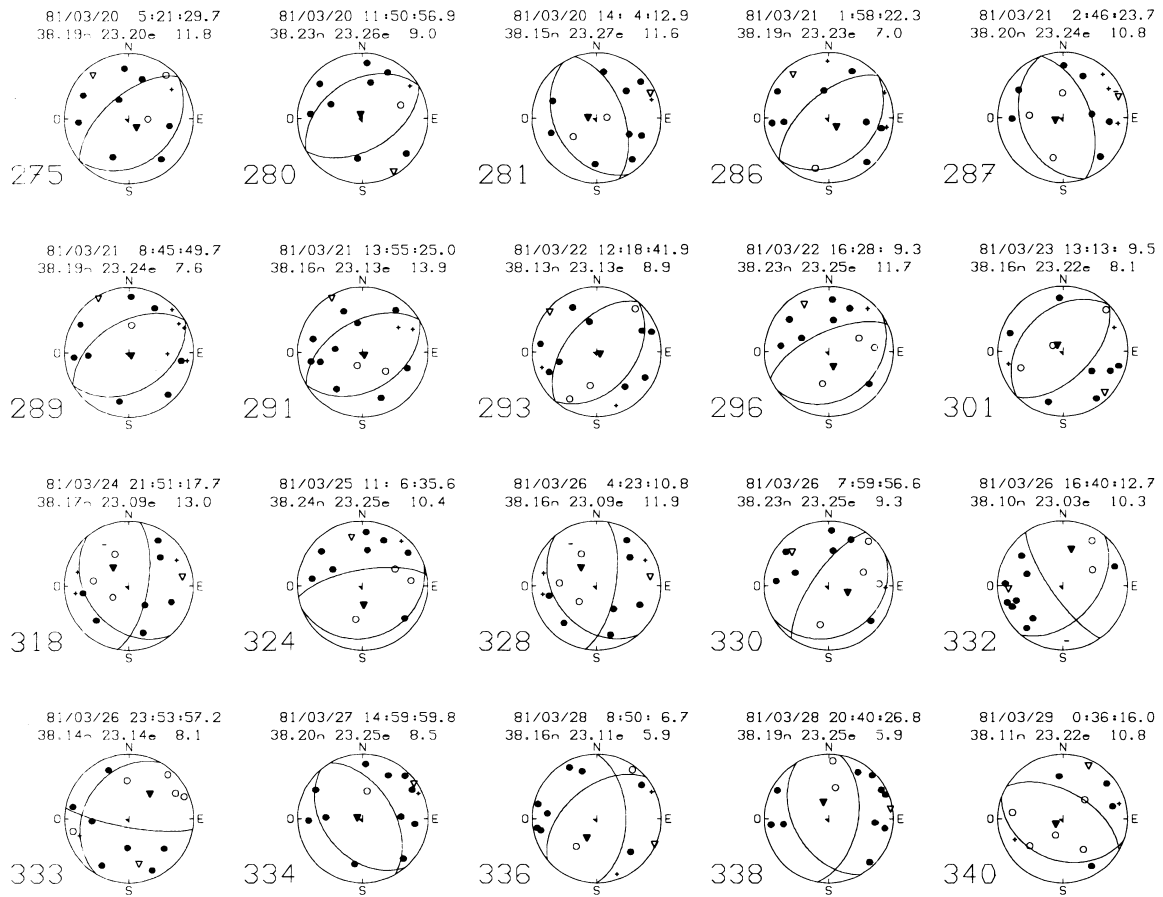


Figure A1. (Continued.)